Experimentele Technieken

in de Hoge Energie Fysica
en verdere toepassingen

Deel 3: Spoor detektoren

Prof. Dr. Albert De Roeck
CERN, Geneva, Switzerland
Universiteit Antwerpen

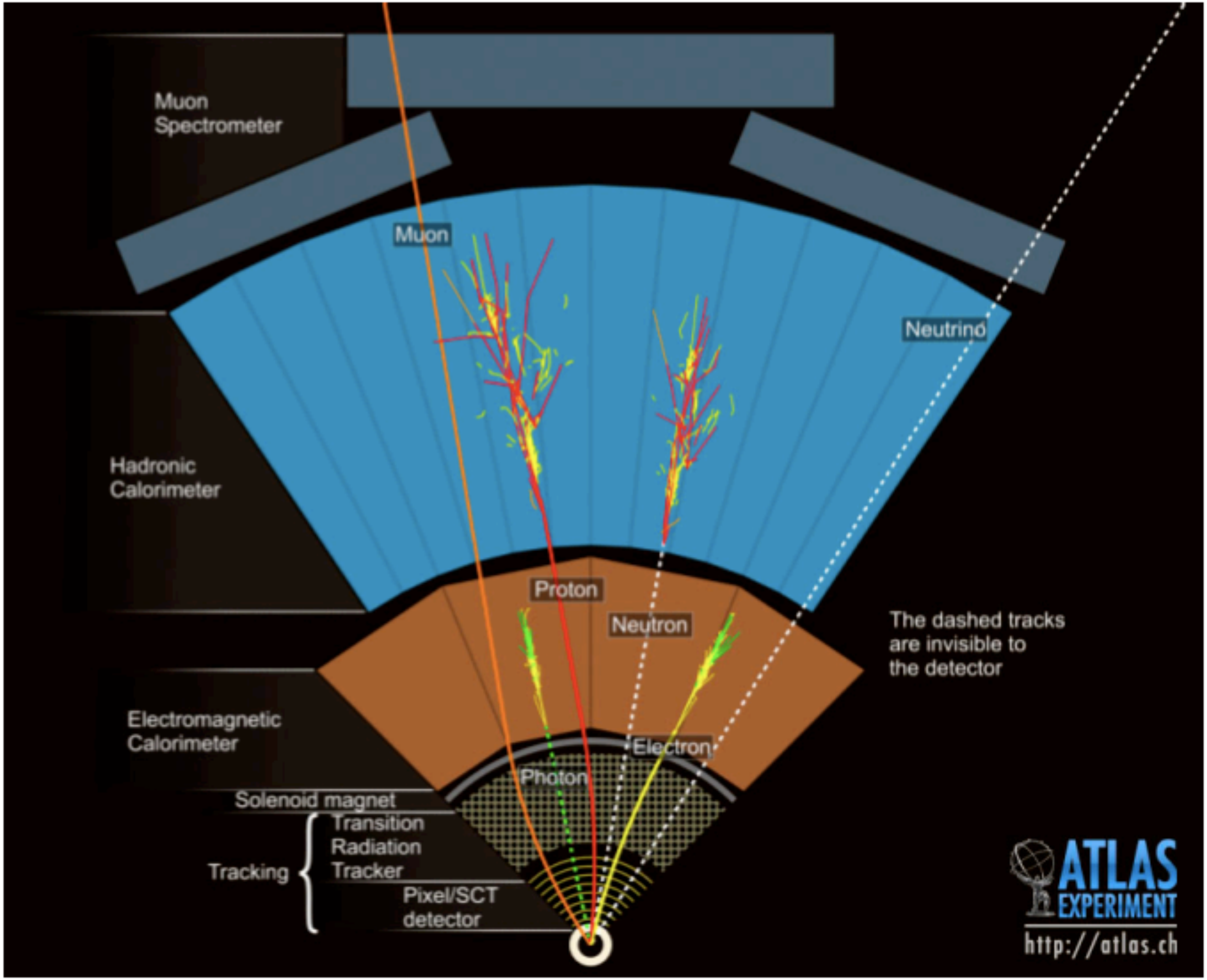
Muon Spectrometer
Muon
Neutrino
Hadronic Calorimeter
Proton
Neutron
The dashed tracks are invisible to the detector
Electromagnetic Calorimeter
Electron
Photon
Solenoid magnet
Transition Radiation Tracker
Tracking
Pixel/SCT detector
ATLAS EXPERIMENT
http://atlas.ch

Interactions with Matter

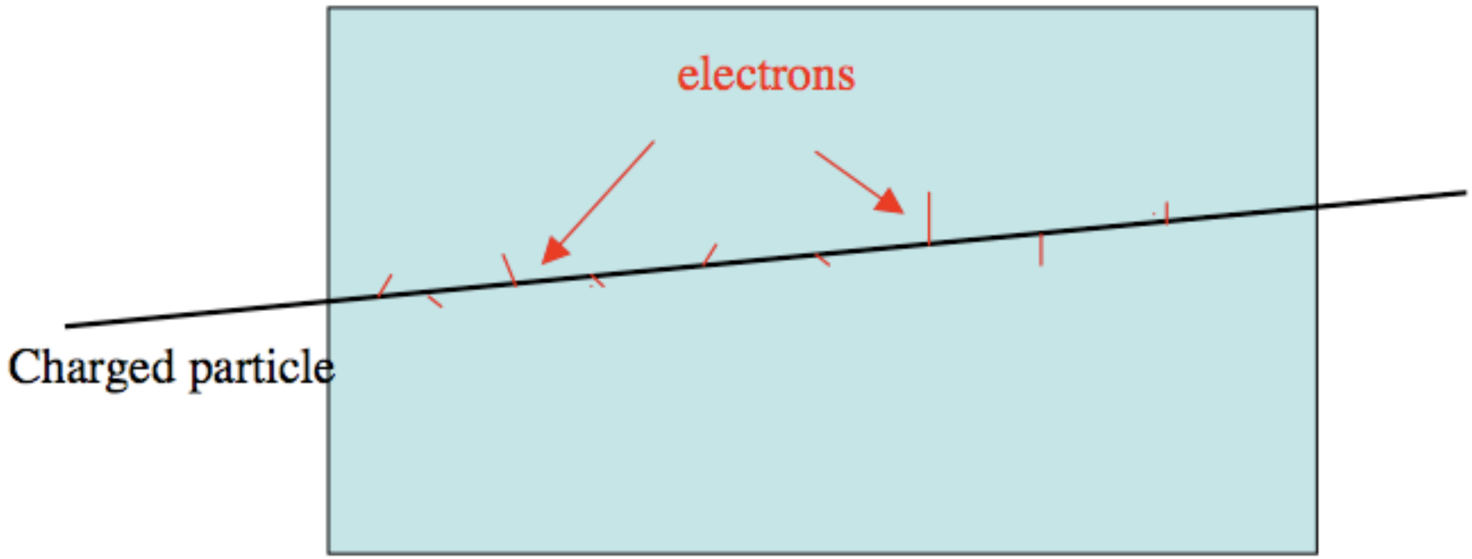

e+ e- collision in the ALEPH Experiment/LEP.

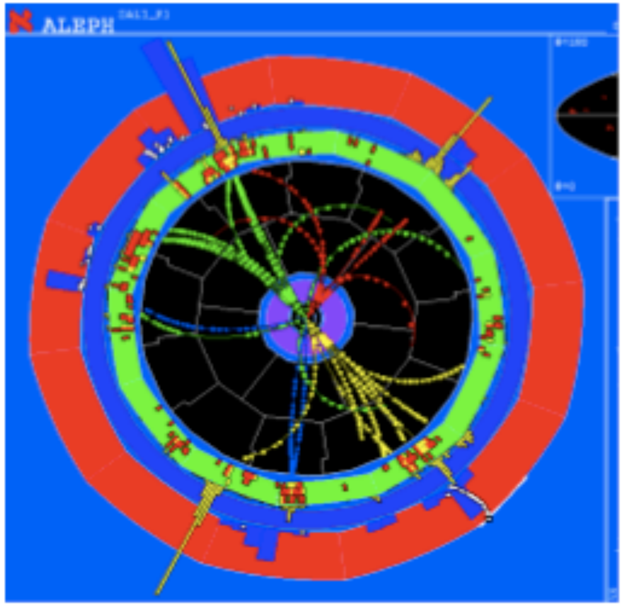

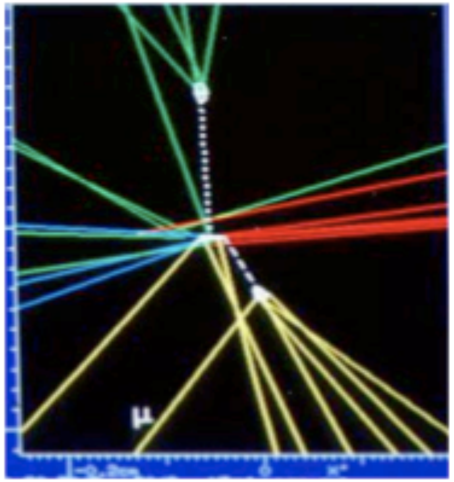

Au+ Au+ collision in the STAR Experiment/RHIC

Up to 2000 tracks

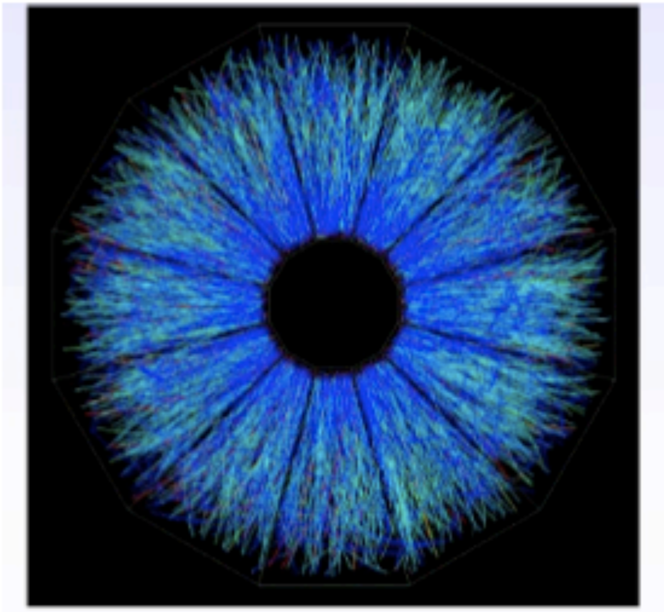

Pb+ Pb+ Kollision in the ALICE Experiment/LHC

Simulation for

Angle Θ=60 to 62º

Up to 40 000 tracks/collision

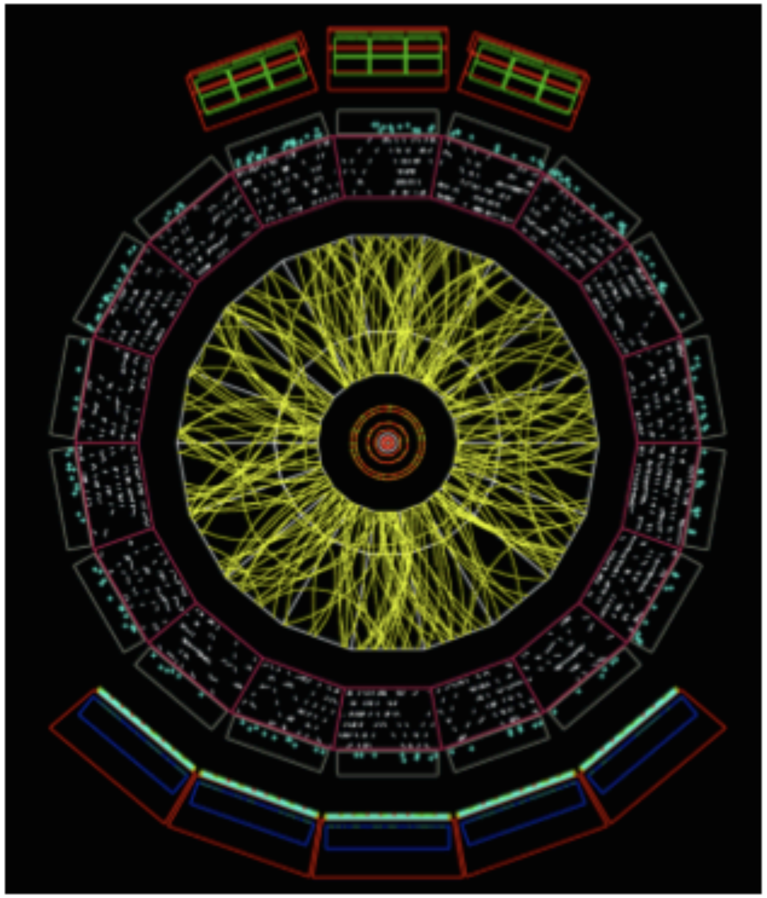

Multiple Scattering

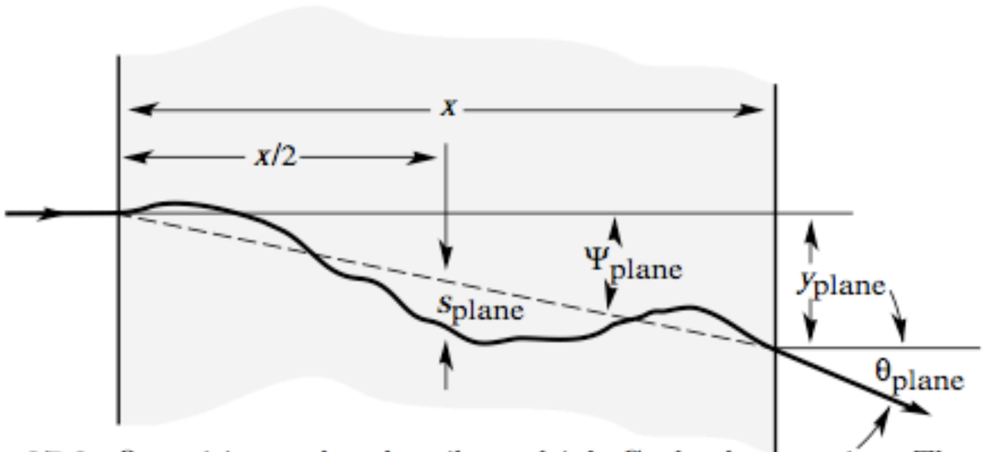

Figure 27.9: Quantities used to describe multiple Coulomb scattering. The particle is incident in the plane of the figure.

$$\psi^{\rm rms}_{\rm plane} = \frac{1}{\sqrt{3}}\,\theta^{\rm rms}_{\rm plane} = \frac{1}{\sqrt{3}}\,\theta_0\ ,$$

$$y^{\rm rms}_{\rm plane} = \frac{1}{\sqrt{3}}\,x\,\theta^{\rm rms}_{\rm plane} = \frac{1}{\sqrt{3}}\,x\,\theta_0\ ,$$

$$s^{\rm rms}_{\rm plane} = \frac{1}{4\sqrt{3}}\,x\,\theta^{\rm rms}_{\rm plane} = \frac{1}{4\sqrt{3}}\,x\,\theta_0\ .$$

A particle which traverses a medium is deflected by small angle Coulomb scattering from nuclei. For hadronic particles also the strong interaction contributes.

The angular deflection after traversing a distance x is described by the Molière theory.
The angle has roughly a Gauss distribution, but with larger tails due to Coulomb scattering.

Defining: $\theta_0 = \theta^{\rm rms}_{\rm plane} = \frac{1}{\sqrt{2}}\theta^{\rm rms}_{\rm space}$

Gaussian approximation:

$$\theta_0 = \frac{13.6\ \text{MeV}}{\beta c p}\, z\, \sqrt{x/X_0}\Big[1 + 0.038\ln(x/X_0)\Big]$$

x/X_0 is the thickness of the material in radiation length.

Momentum Measurements in B-field

The momentum is measured from the sagitta s, which gives the curvature ρ of the track in the magnetic field.

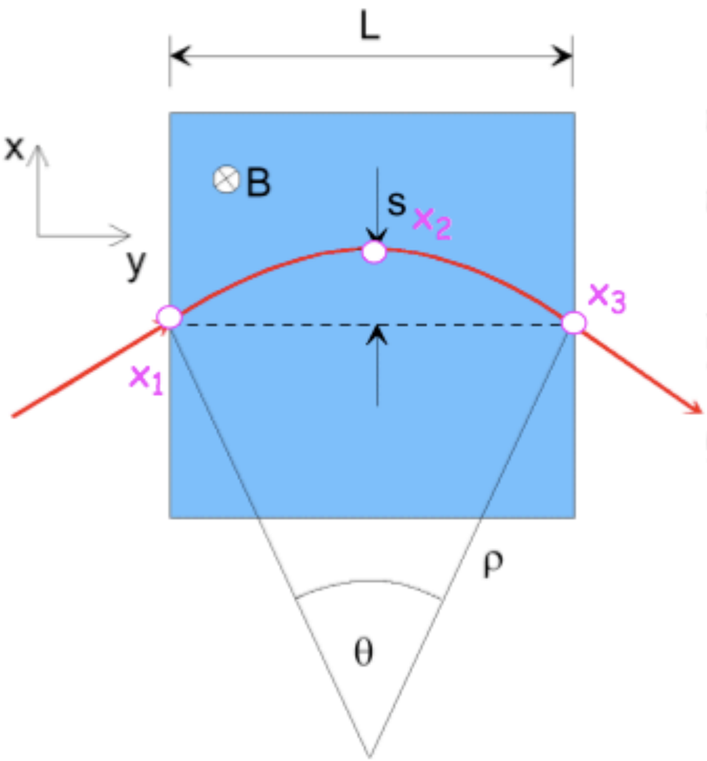

Transverse momentum:

$$p_T = qB\rho$$

$$p_T[GeV] = 0.3\ B[T]\ \rho[m]$$

$$\frac{L/2}{\rho} = \sin\frac{\theta}{2} \approx \frac{\theta}{2}\ \text{(for small } \theta) \Rightarrow \theta \approx \frac{L}{\rho} = \frac{0.3BL}{p_T}$$

$$s = \rho(1-\cos\frac{\theta}{2}) \approx \rho\left(1-(1-\frac{1}{2}\frac{\theta^2}{4})\right) = \rho\frac{\theta^2}{8} \approx \frac{0.3BL^2}{8p_T}$$

Examples

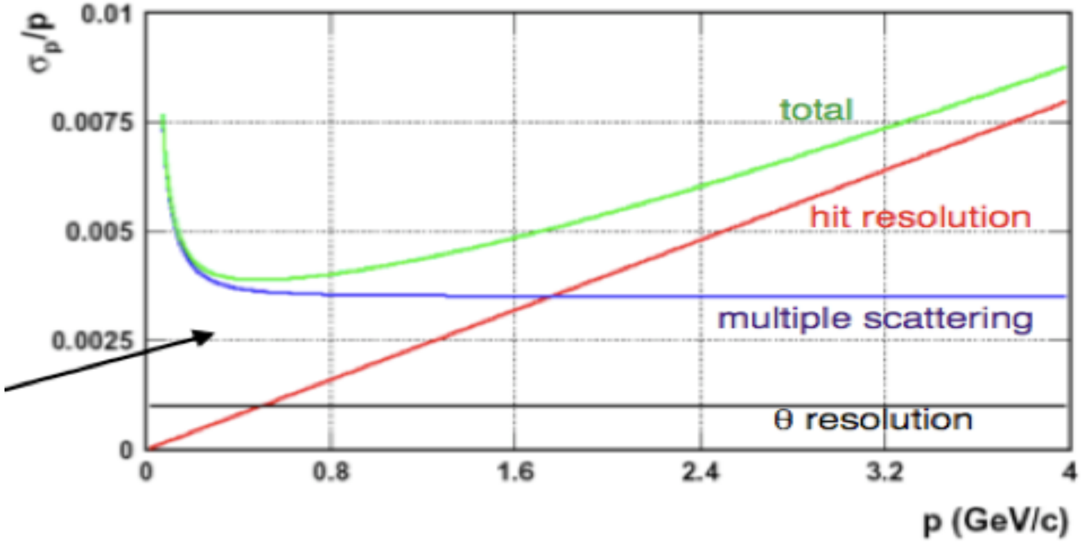

Drift and Diffusion in Gases

from L.Ropelewski

E=0 thermal diffusion $\langle v \rangle_t = 0$

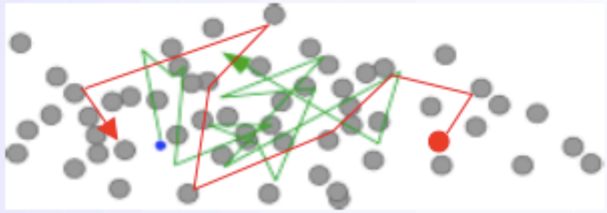

E>0 charge transport and diffusion $\langle v \rangle_t = v_D$

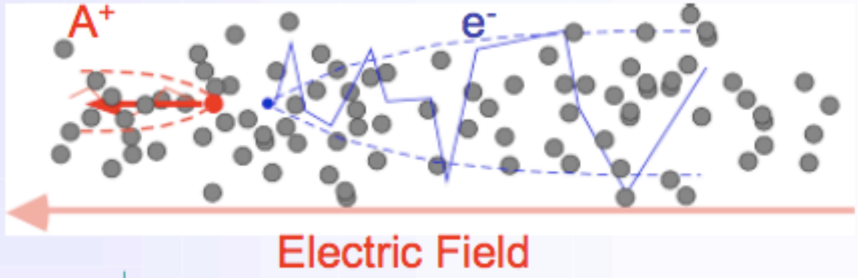

Electron swarm drift

Drift velocity

Diffusion

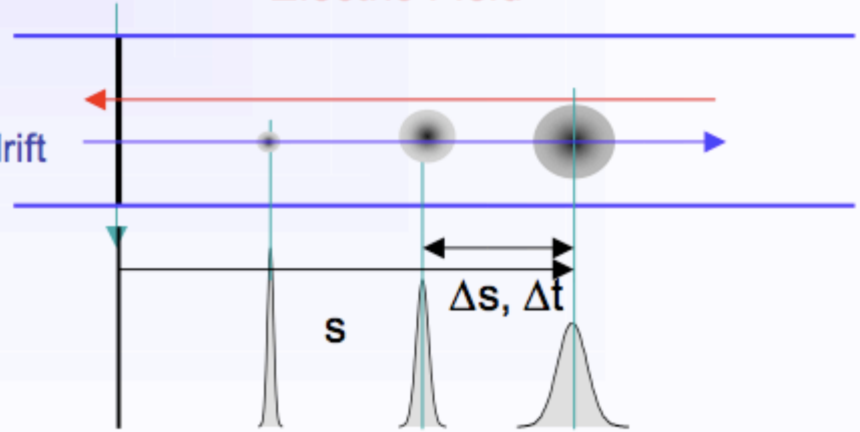

$$v_D = \frac{\Delta s}{\Delta t}$$

$$\sigma_x = \sqrt{2Dt} = \sqrt{2D\frac{s}{v_D}}$$

Lorentz Angle in a magnetic Field

Lorentz angle (deflection angle of drift electrons due to magnetic field)

$$\tan\alpha = v_{drift}\,\frac{B}{E}$$

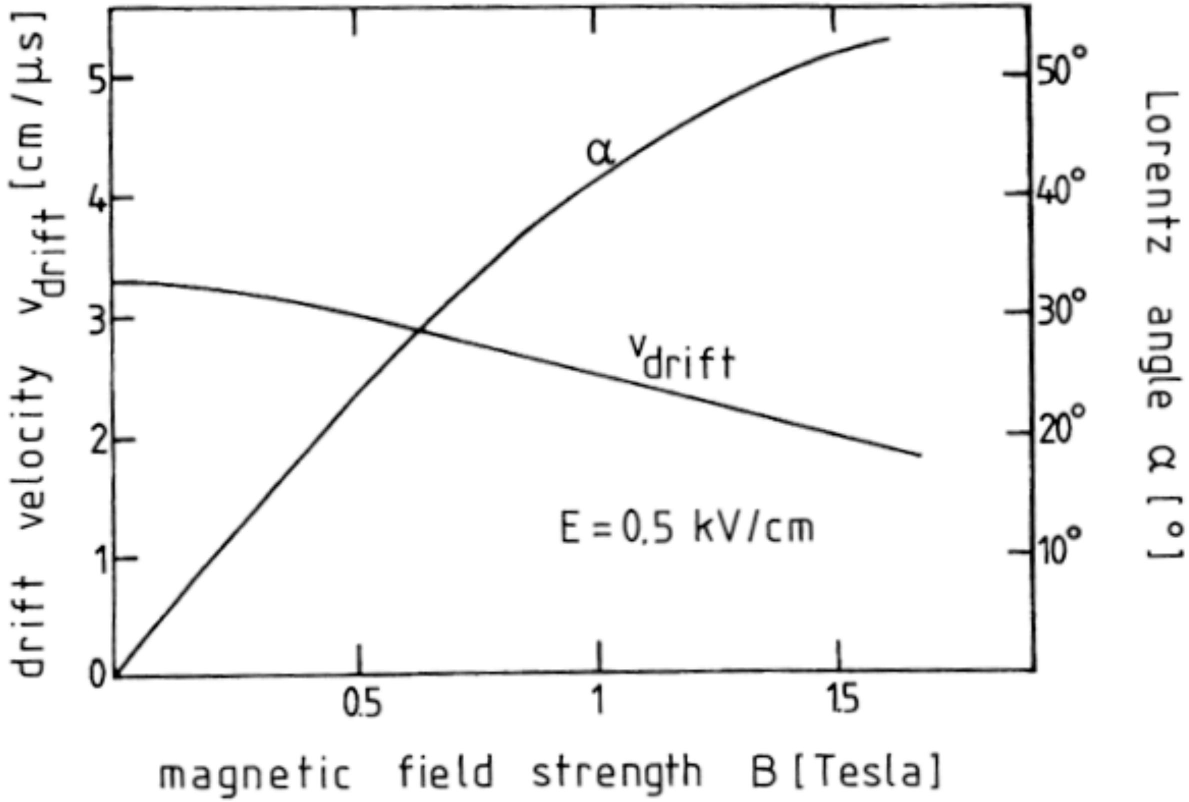

Fig. 1.21. Dependence of the electron drift velocity $\vec{v}_{\rm drift}$ and the Lorentz angle α on the magnetic field for low electric field strengths (500 V/cm) in a gas mixture of argon (67.2 %), isobutane (30.3 %) and methylal (2.5 %) [51, 95].

History of Tracking: Cloud Chambers

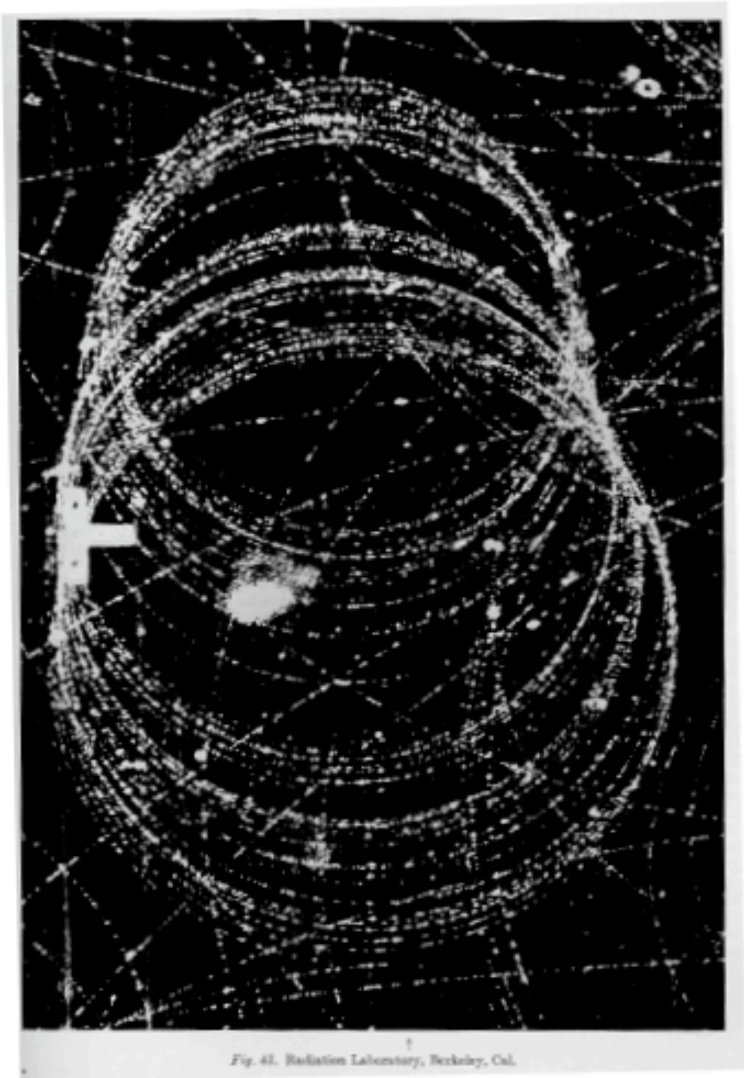

Fast electron in a magnetic field at the Bevatron, 1940

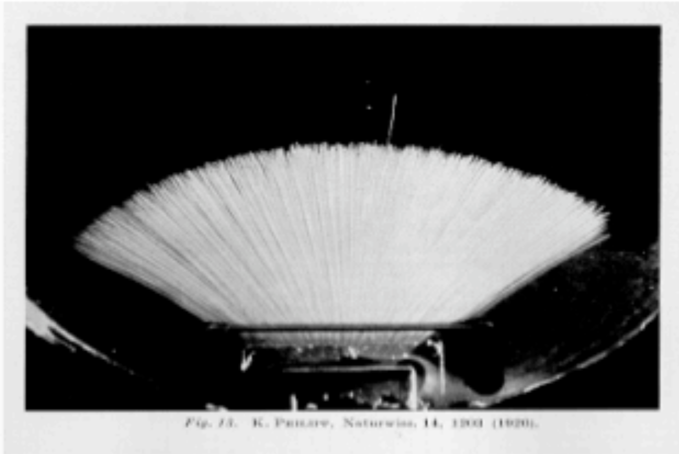

α-particles in air.

In cloud chambers a charged particle causes condensation of a supersaturated gas.

The picture (left) shows and electron with 16.9 MeV initial energy.

It spirals about 36 times in the magnetic field.

Nobel prizes related to cloud chamber development:
C. T. R. Wilson, 1927
P.M.S. Blackett, 1948 (triggered chambers)

History of Tracking: Emulsion

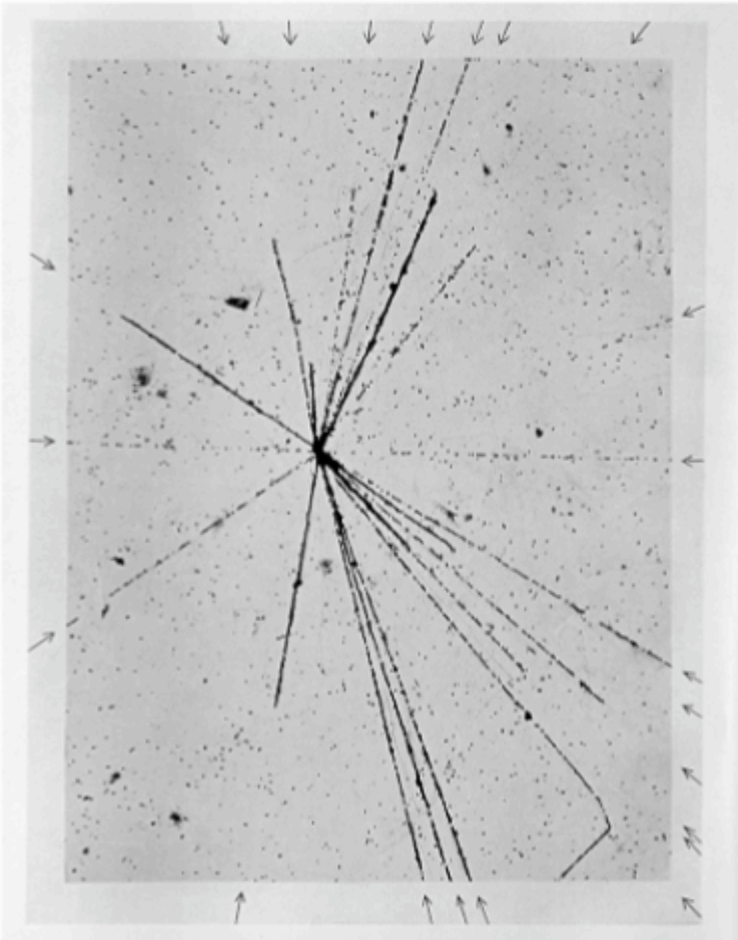

'EXPLOSIVE' DISINTEGRATION OF A NUCLEUS

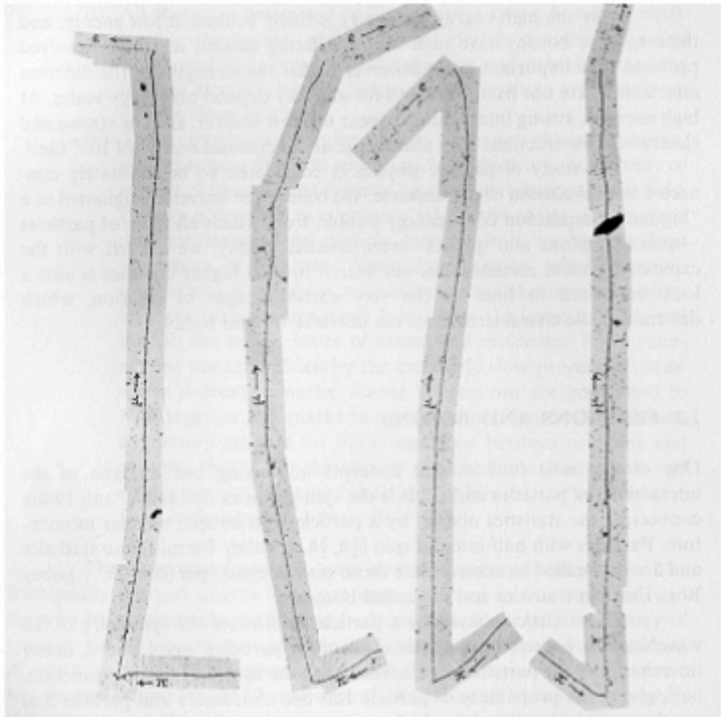

Discovery of muon and pion

Emulsion detectors are still used today: Opera experiment at Gran Sasso for the identification of tau decays.

History of Tracking: Bubble Chambers

Cloud chamber: supersaturating a gas with a vapor.

Bubble chamber: superheated liquid. Invented by Donald A. Glazer, Nobel Prize 1960.

A particle depositing energy along it's path makes the liquid boil and forms bubbles.

The 80-inch Bubble Chamber

BNL, First Pictures 1963, 0.03s cycle

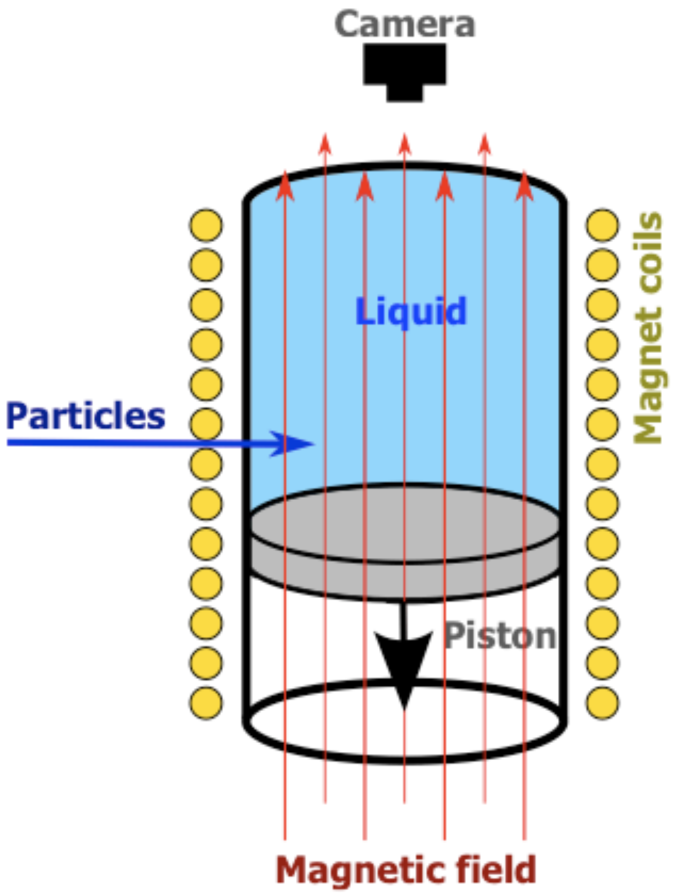

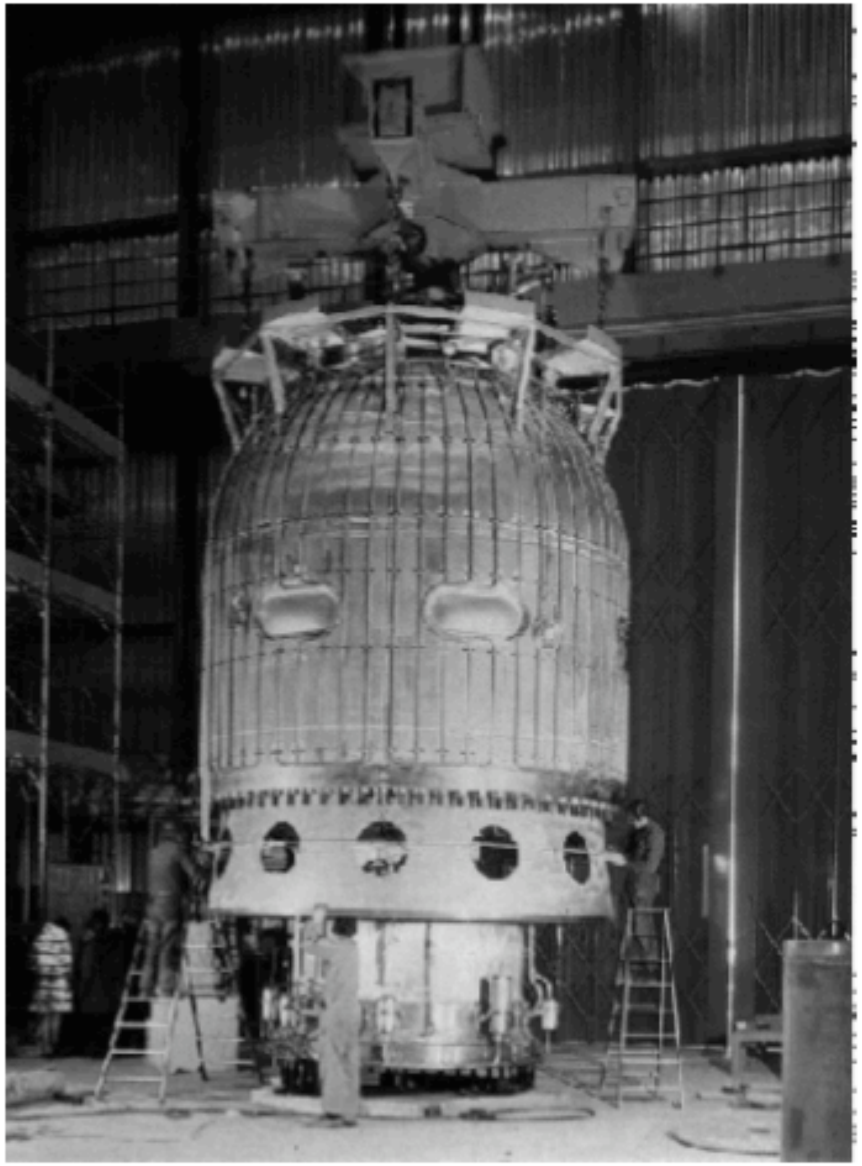

Can be seen outside the Microcosm Exhibition

3.7 meter hydrogen bubble chamber at CERN, equipped with the largest superconducting magnet in the world at that time.

During its working life from 1973 to 1984, the "Big European Bubble Chamber" (BEBC) took over 6 million photographs.

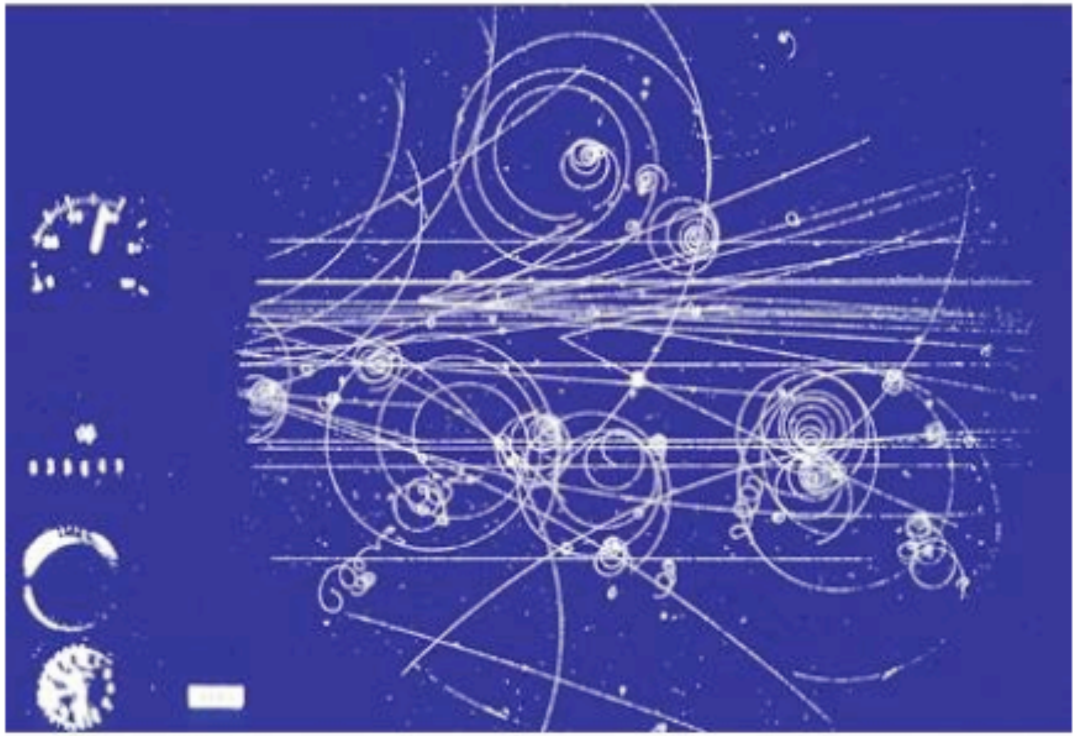

Bubble Chambers

The excellent position (5μm) resolution and the fact that target and detecting volume are the same (H chambers) makes the Bubble chamber almost unbeatable for reconstruction of complex decay modes.

The drawback of the bubble chamber is the low rate capability (a few tens/ second). E.g. LHC 10^9 collisions/s.

The fact that it cannot be triggered selectively means that every interaction must be photographed.

Analyzing the millions of images by 'operators' was a quite laborious task.

That's why electronics detectors took over in the 70ties.

Ionization Chambers

- simplest Gas Detector
- Basically a Capacitor
- Also possible with liquids and solids

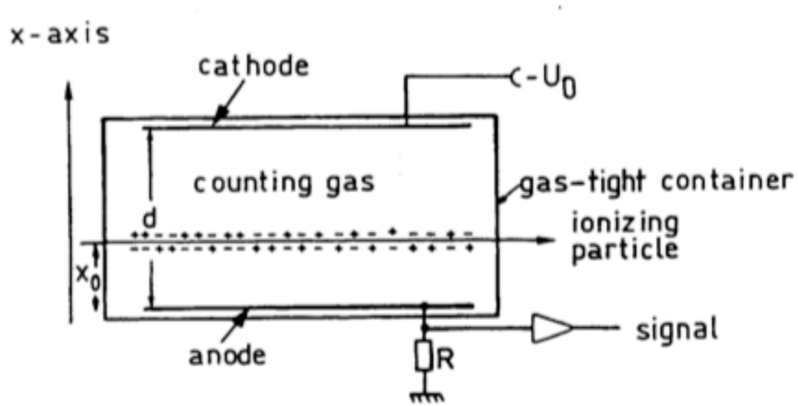

- Ionization (electrons and ions) drift to anode and cathode

If time constant of RC is large enough: Integrated signal $\propto$ Ionization loss

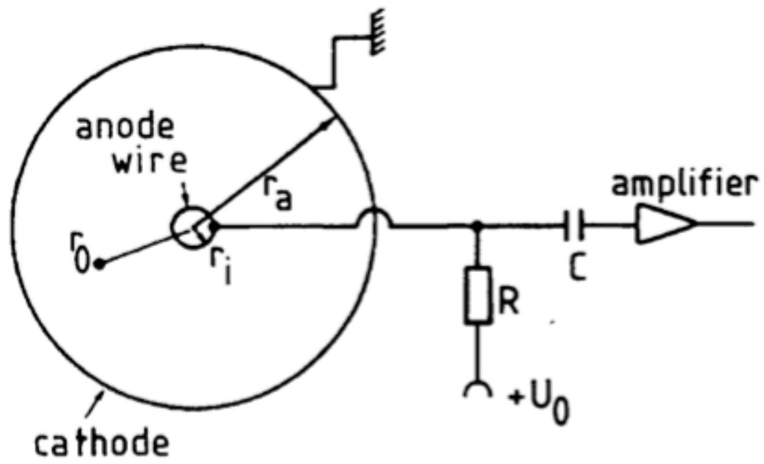

Ionization Chambers

SWPC OPERATION MODE

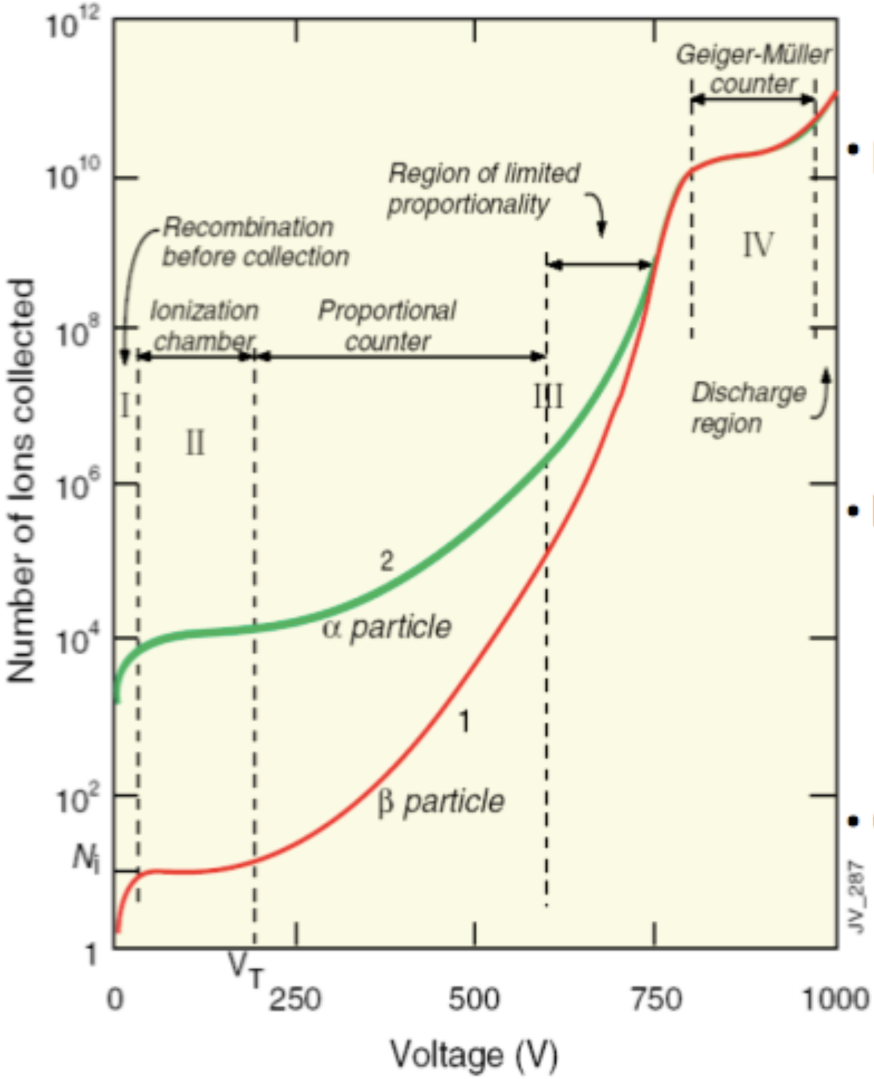

- ionization mode
  - full charge collection
  - no multiplication
  - gain ~ 1
- proportional mode
  - multiplication of ionization
  - signal proportional to ionization
  - measurement of dE/dx
  - secondary avalanches have to be quenched;
  - gain ~ $10^4 – 10^5$
- limited proportional mode (saturated, streamer)
  - strong photoemission
  - secondary avalanches
  - requires strong quenchers or pulsed HV; gain ~ 10^{10}
- Geiger mode
  - massive photoemission; full length of the anode wire affected;
  - discharge stopped byHV cut

Proportional Chamber: Single Wire

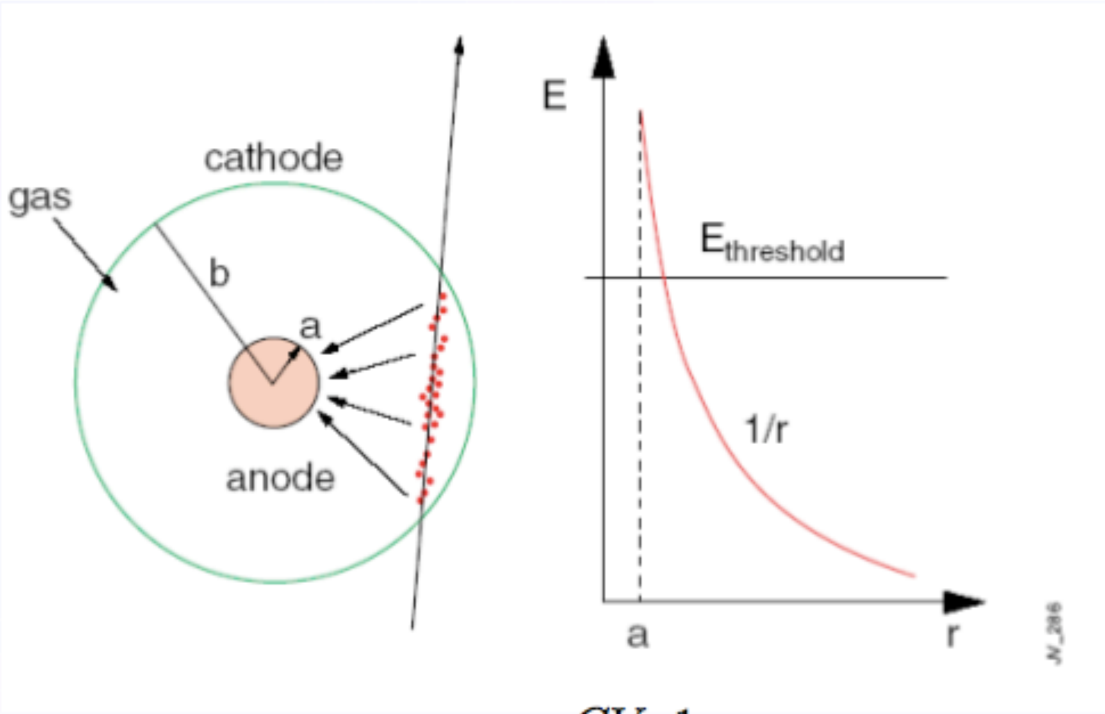

Electric field: $$E(r) = \frac{CV_0}{2\pi\epsilon_0}\frac{1}{r}$$

Potential: $$V(r) = \frac{CV_0}{2\pi\epsilon_0}\ln\frac{r}{a}$$

V_0 = voltage between anode-cathode

Capacitance per length $$C = \frac{2\pi\epsilon}{\ln(b/a)}$$

Electrons produced by ionization drift to the anode wire.

Avalanche:

- Close to the wire (⌀ about few tens of μm) the E-field is very large (> 10 kV/cm).
- Between collisions electrons gain enough energy to ionize gas.
- Exponential increase of number of electron/ion pairs (gas amplification)

$$n = n_0\ e^{\alpha(E)x}$$

α is the first Townsend coefficient.

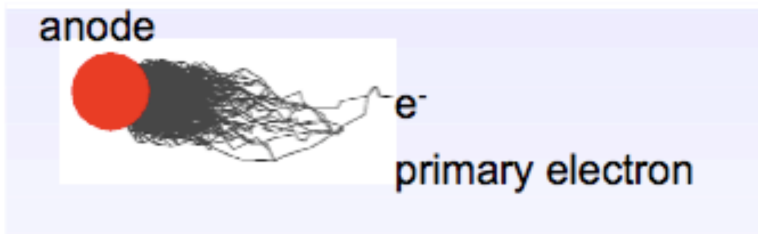

Proportional Chambers

- Like Ionization chamber, but smaller wire and/or higher voltage
- Charge multiplication close to wire ($E \propto 1/r$)
- Electrons gain enough energy between collisions to ionize themselves.

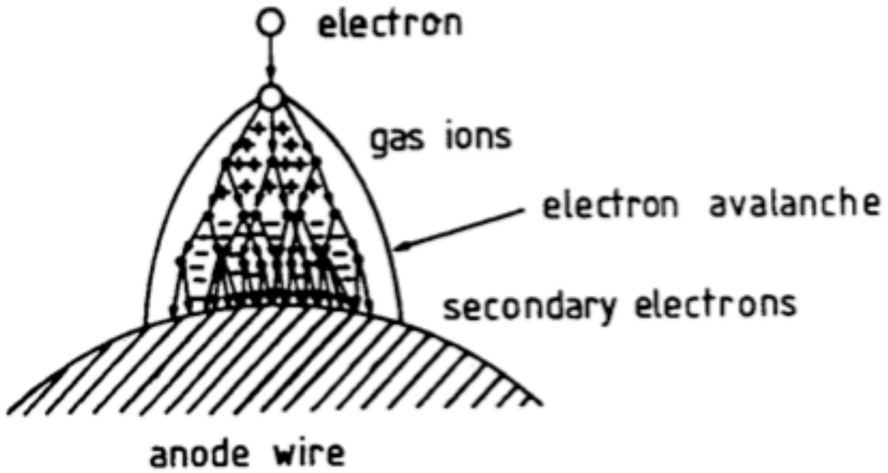

- Proportional: Gas amplification constant
  $\rightarrow$ Signal $\propto$ primary ionization

Proportional Chambers

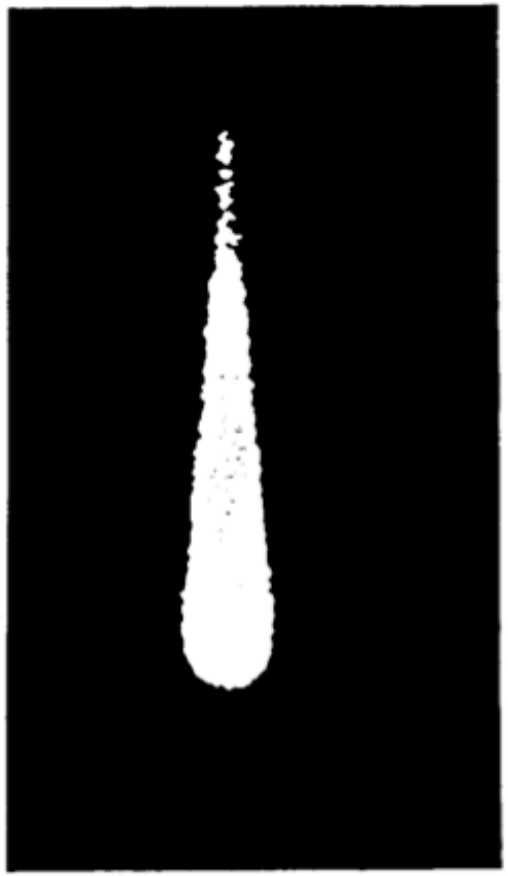

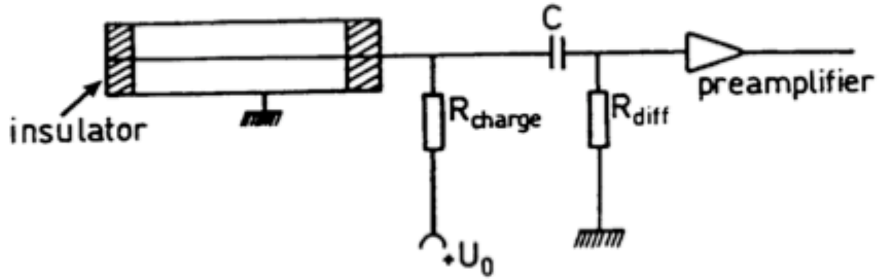

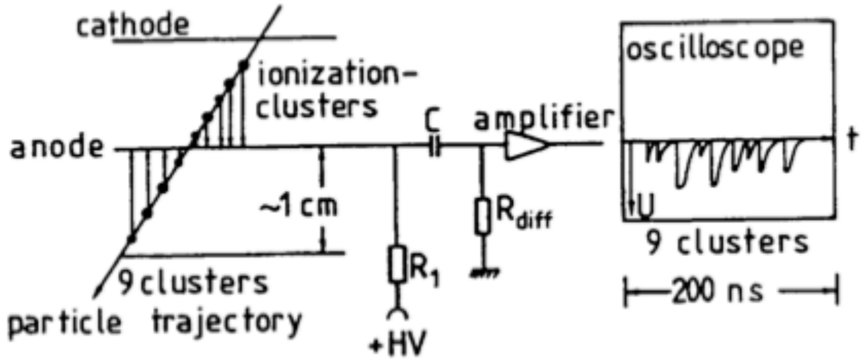

Spark Chamber

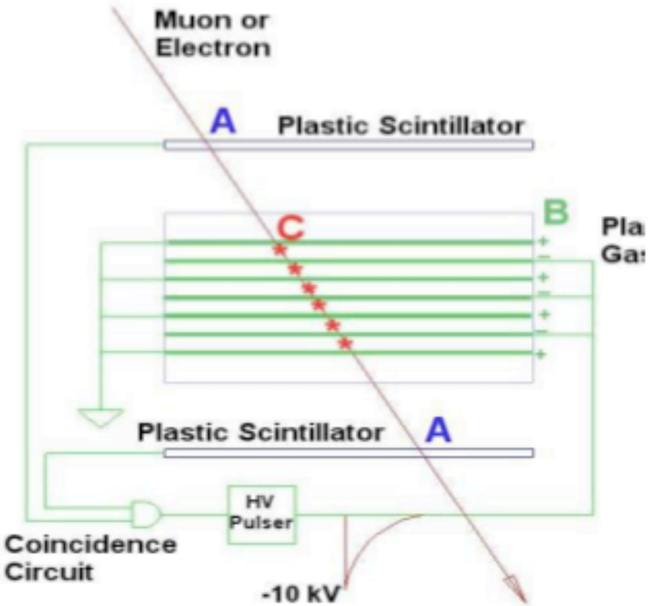

The Spark Chamber was developed in the early 60ies.

Schwartz, Steinberger and Lederman used it in discovery of the muon neutrino

A charged particle traverses the detector and leaves an ionization trail.

The scintillators trigger an HV pulse between the metal plates and sparks form in the place where the ionization took place.

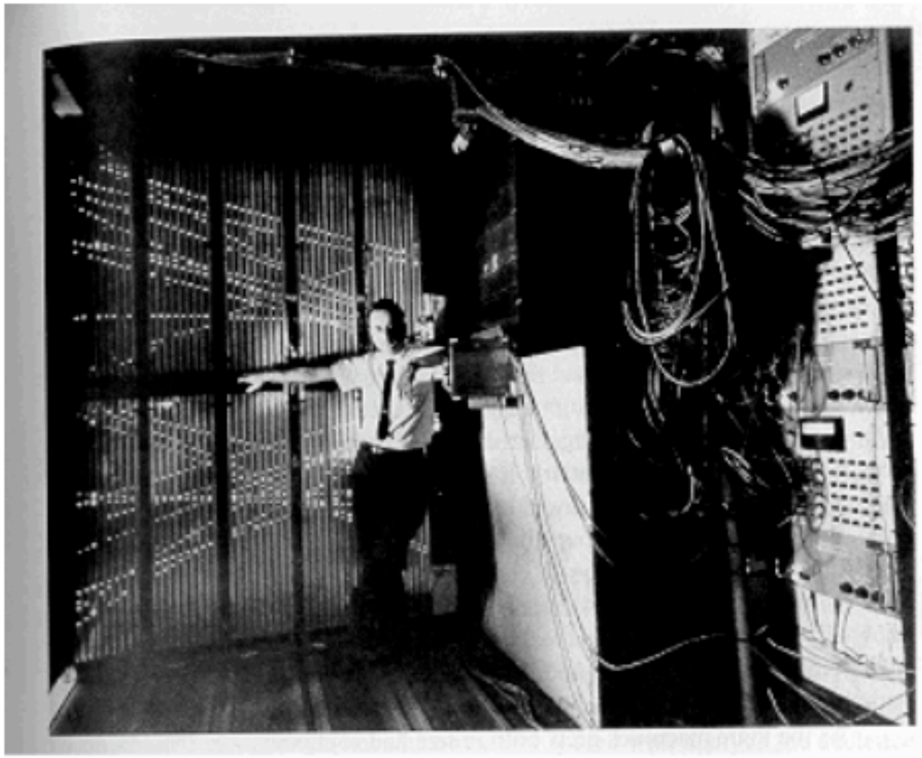

Geiger-Muller Counter

- Even higher voltage
- Copious production of photons in avalanche
- Photons make more ionization by photoelectric effect
- Also far away from original avalanche

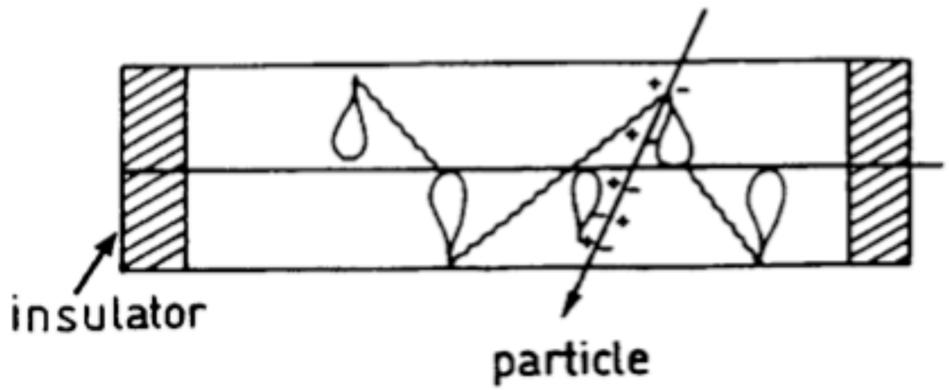

- To stop discharge:
  - Make charge resistor big enough so voltage drops enough (quenching by resistor)
  - Add alcohols (methylal, ethylaclohol) or hydrocarbons (methan, ethane, isobutane) to counting gas (usually argon):
    Absorb UV photons, reduce free path

Multi-Wire proportional Chamber

from L. Ropelewski

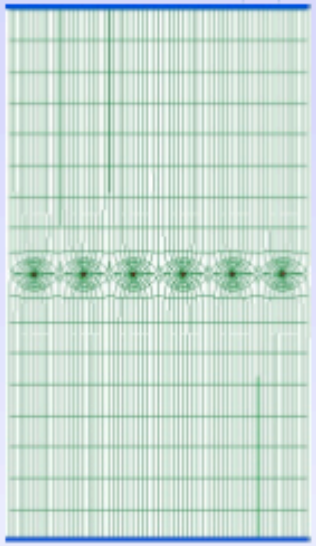

Simple idea to multiply SWPC cell : Nobel Prize 1992

First electronic device allowing high statistics experiments !!

Typical geometry

5mm, 1mm, 20 μm

Normally digital readout :

spatial resolution limited to

$$\sigma_x \approx \frac{d}{\sqrt{12}}$$

for d=1 mm
σ_x = 300 μm

$$\langle x^2 \rangle = \frac{\int_0^{d/2} x^2 dx}{\int_0^{d/2} dx} = \frac{2}{d} \frac{x^3}{3} \Big|_0^{d/2} = \frac{d^2}{12}$$

First large size MWPC

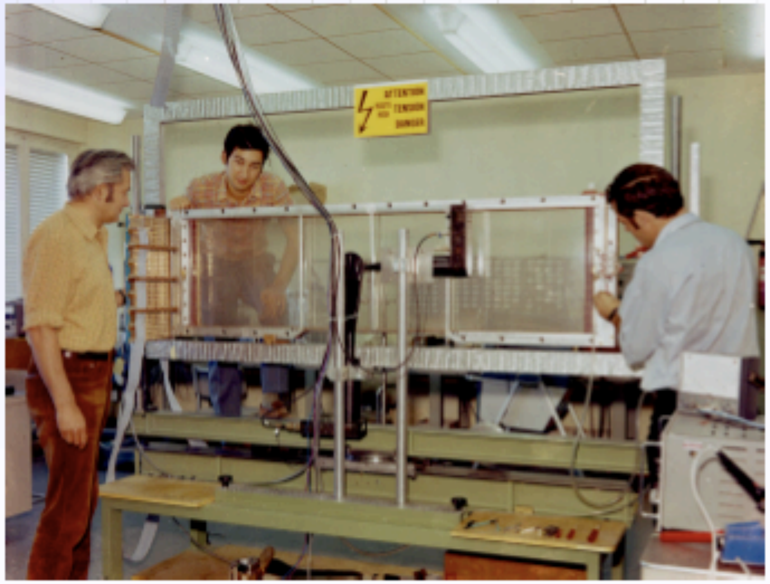

G. Charpak, F. Sauli and J.C. Santiard ,1970

Multi-Wire Propotional Chambers

- George Charpak, beginning of 1960's, Nobel Price 1992
- Typical wire distance d: a few mm ($> 0.8\,\text{mm}$)
- Typical wire diameter: $10\,\mu\text{m} - 30\,\mu\text{m}$
- Sizes: up to square meters. Limited by wire tension and electrostatic repulsion.
- Electronic: Discriminator (threshold).
- Resolution: $\sigma(x) = d/\sqrt{12}$
- space information only in one dimension
- Rotate second identical module for other dimension
- Segmented cathode readout for other dimension

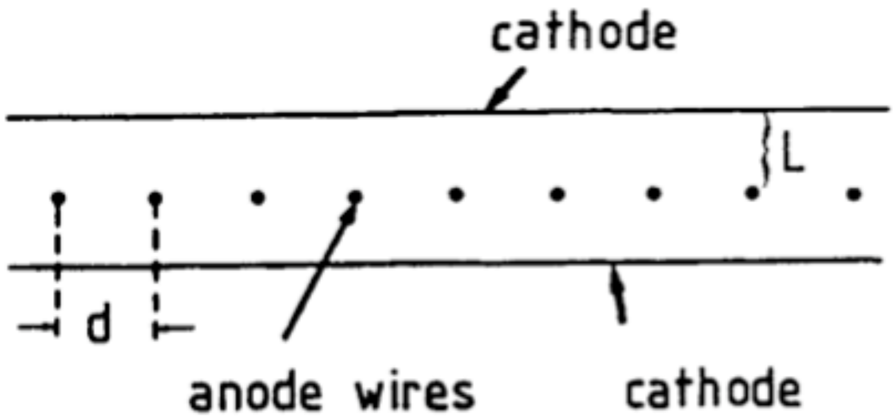

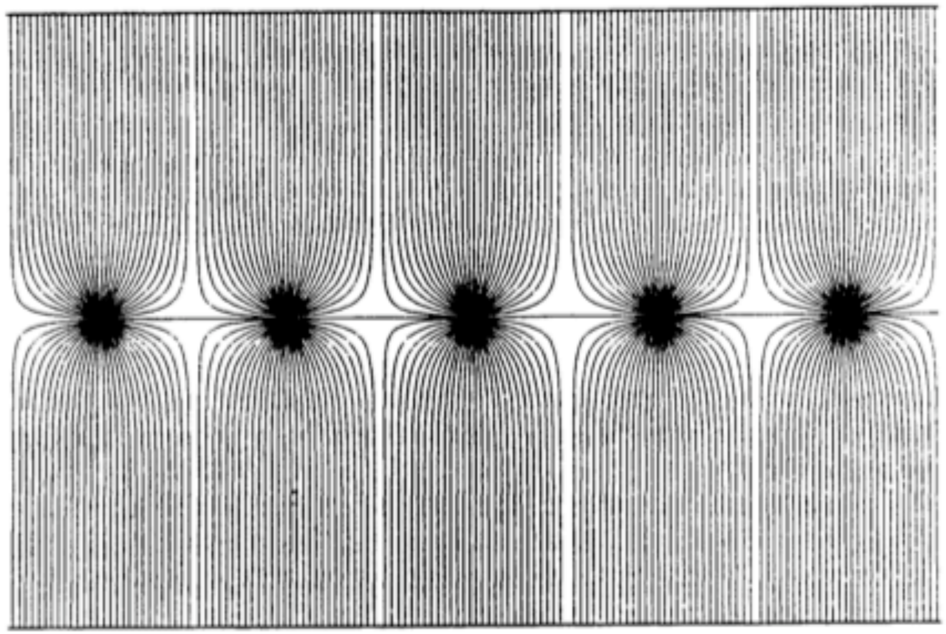

Multi-wire Proportional Chambe

Two coordinates (x,y) of the track hit can be determined from the position of the anode wire and the signal induced on the cathode strips (or wires).

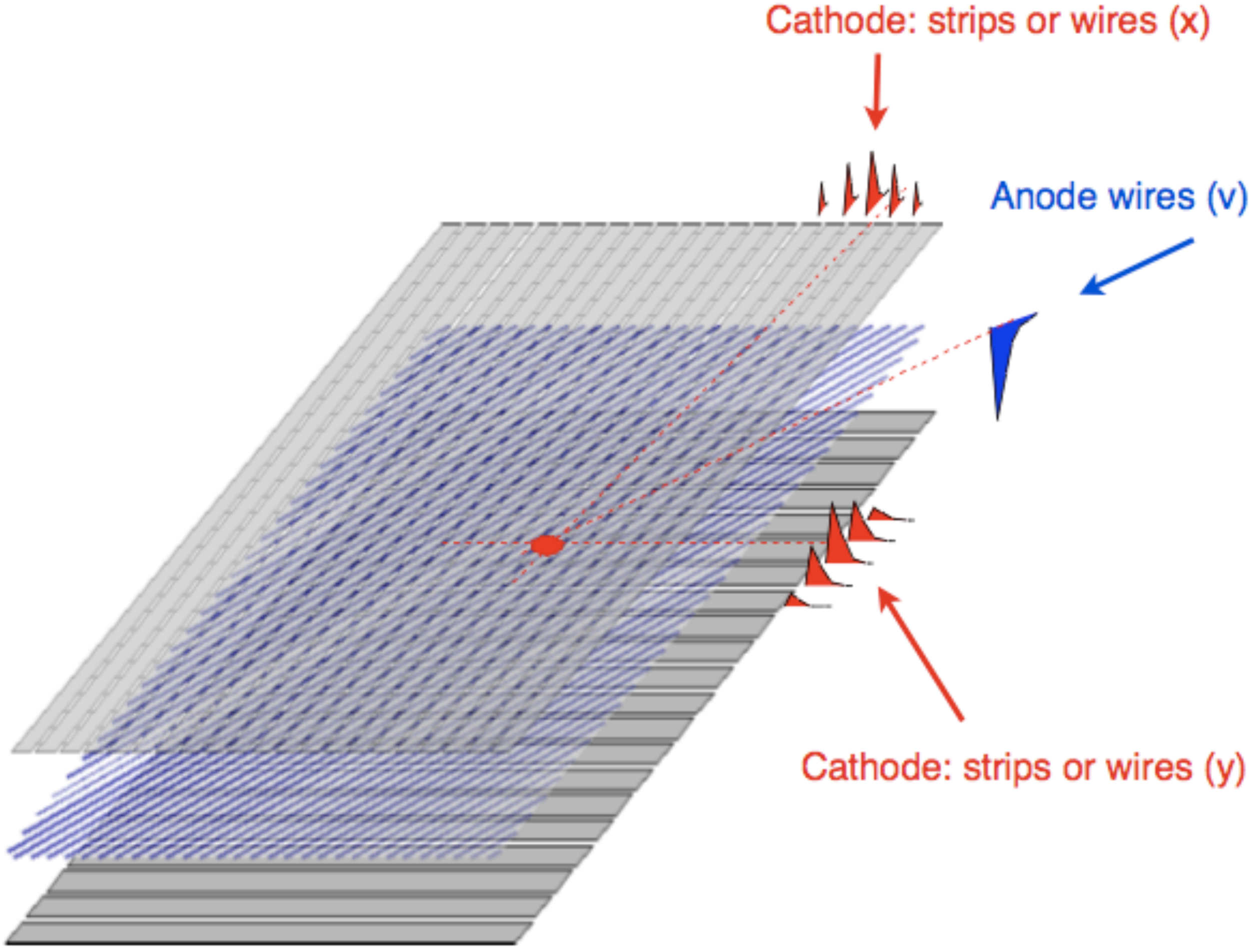

MWPC: Experimental set-up

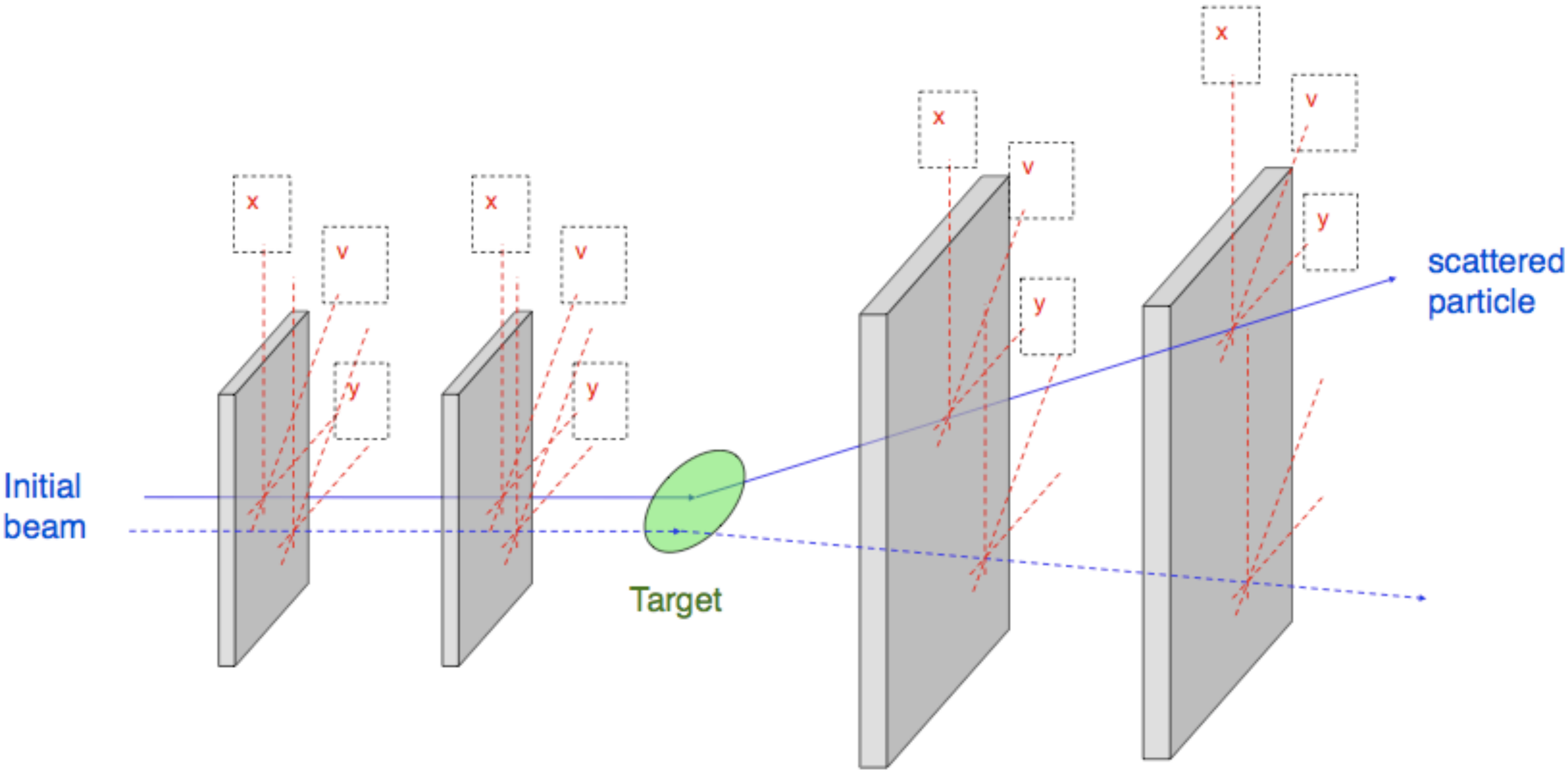

With this experimental set-up based on MWPC an event rate of about 100 000 Hz can be processed.
The position resolution in each layer is about 1 mm.

MWPC with many wire planes. 1985

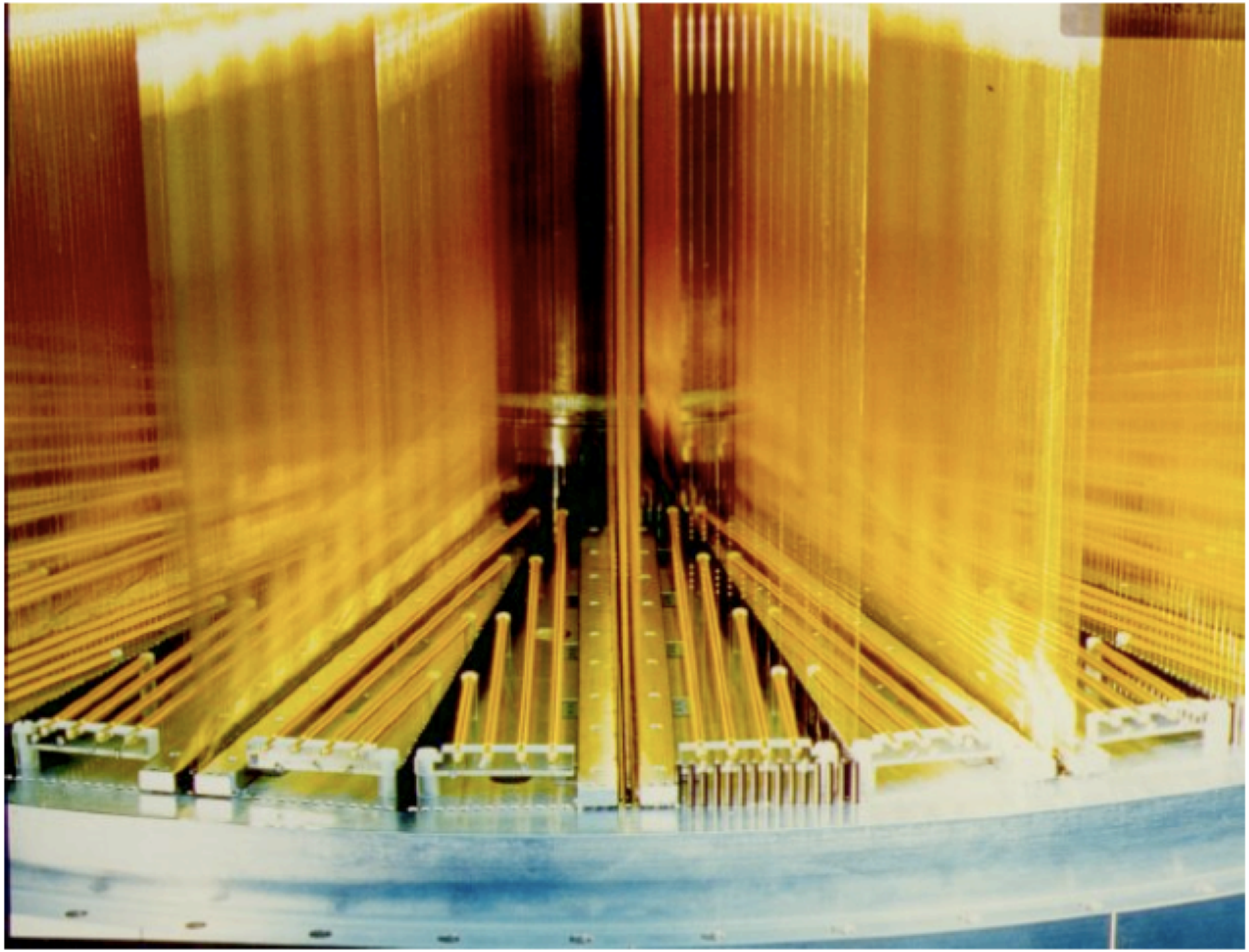


SENSOR HEAD
#6
SENSOR HEAD
#7

Cathode Strip Chambers

from L. Ropelewski

Precise measurement of the second coordinate by interpolation of the signal induced on pads.
Closely spaced wires makes CSC fast detector.

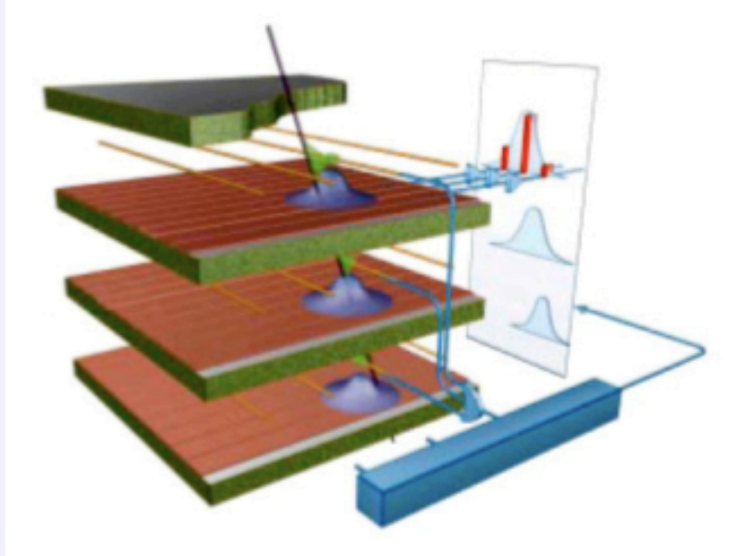

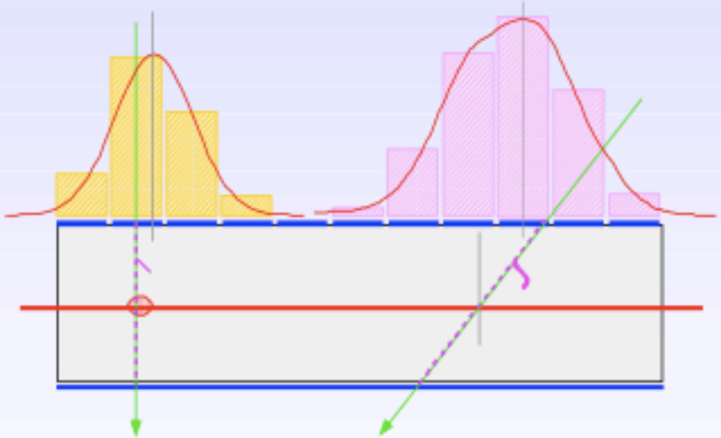

Center of gravity of induced signal method.

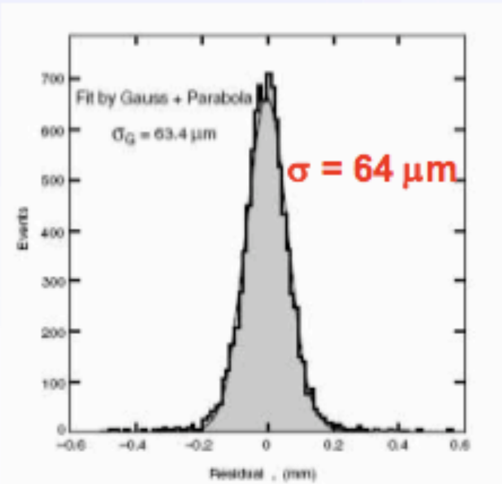

Space resolution

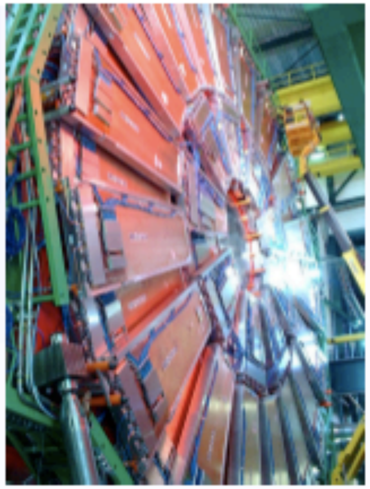
CMS

Resistive Plate Chambers

from L. Ropelewski

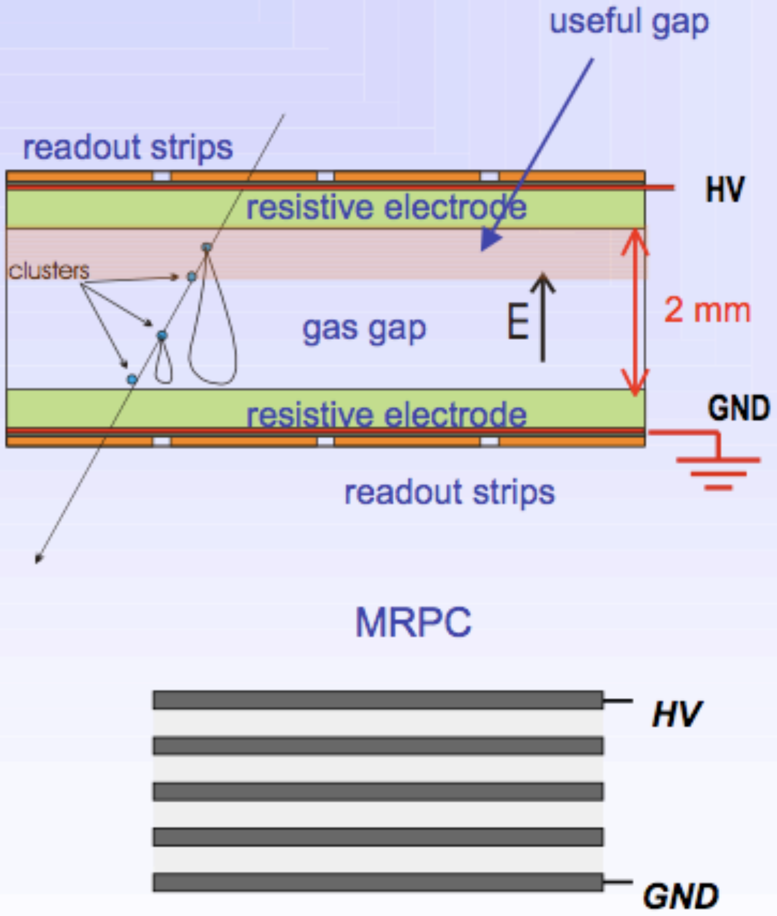

Multigap RPC - exceptional time resolution suited for the trigger applications

Rate capability strong function of the resistivity of electrodes in streamer mode.

A. Akindinov et al., NIM A456(2000)16

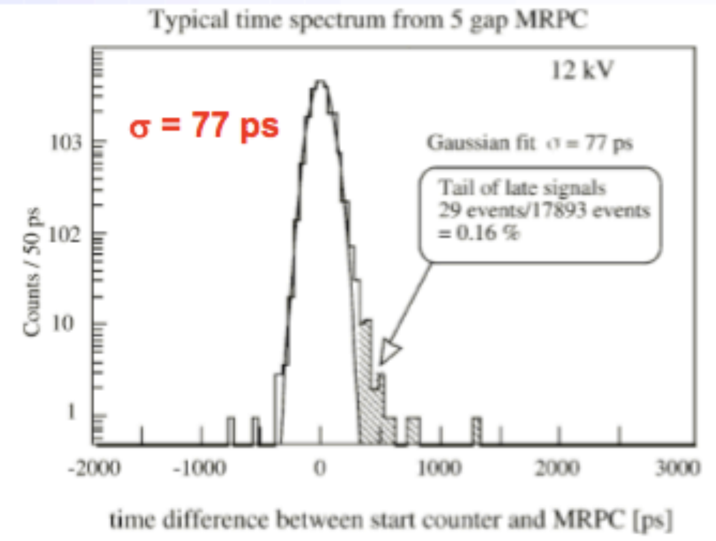

Time resolution

Driftchamber

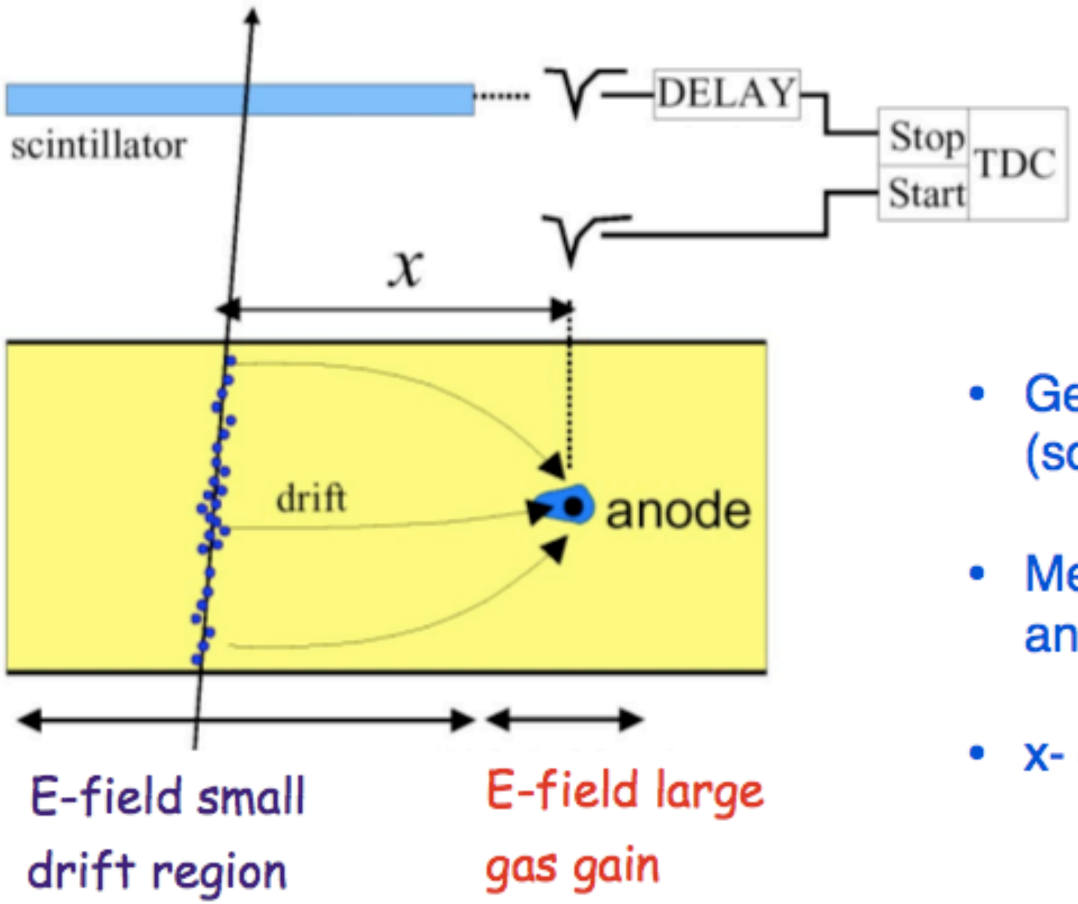

TDC: Time to Digital Converter

- Get external time reference t_0 (scintillator)
- Measure arrival time of electrons at anode t_1
- x- coordinate given by $x = \int_{t_0}^{t_1} v_D(t)\, dt$
- advantage of drift chamber: much larger sensitive volume per readout channel.

Planar Drift Chambers

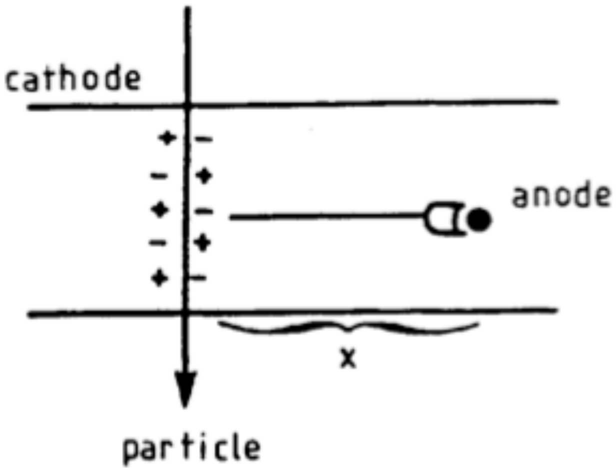

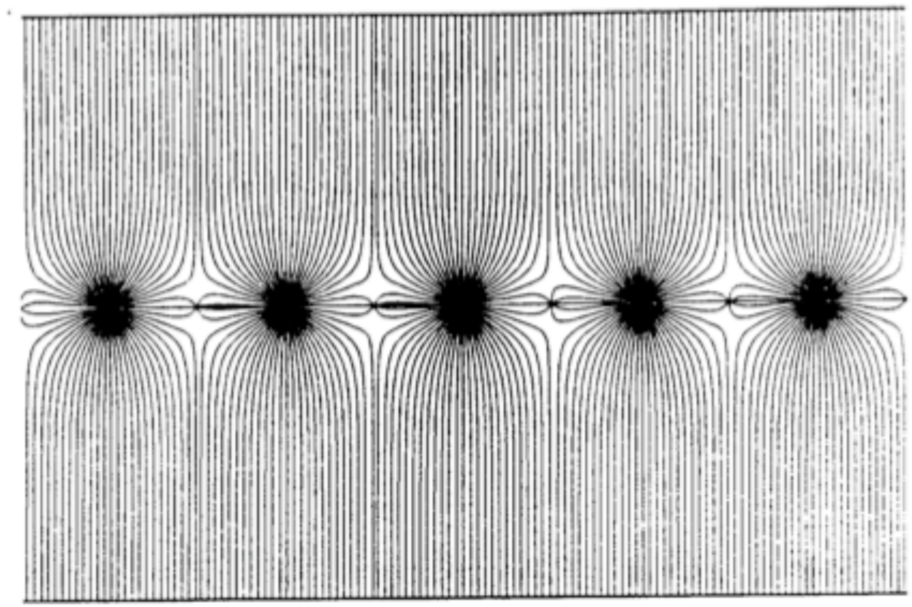

- Heintze, Walenta, ≈ 1968, also others.
- Make wires further apart
- use drift time to wire as additional information
- additional potential wire
- drift distances several cm
- resolution: limited by diffusion.
  small chambers: $\sigma > 20\,\mu$m
  larger chambers a few 100 μm

Driftchamber

- Use graded potential to get uniform drift field.
- Gas amplification near anode wire.
- Position resolution (σ= 50 - 200 μm)
  - v(t) distortions near wire
  - ionisation fluctuations
  - diffusion
  - electronic noise

drift cell

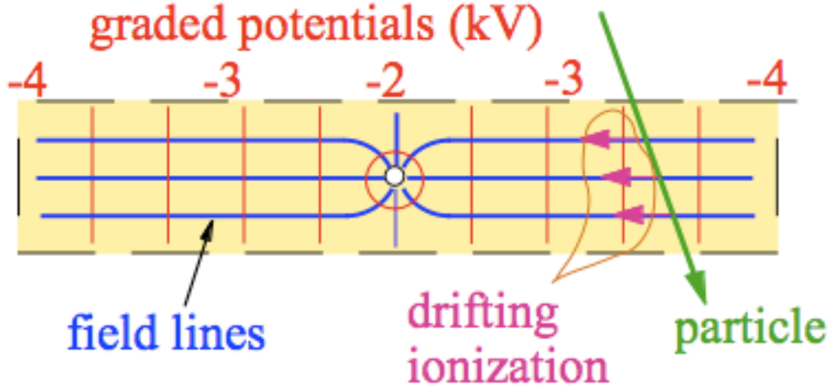

CDF muon chambers

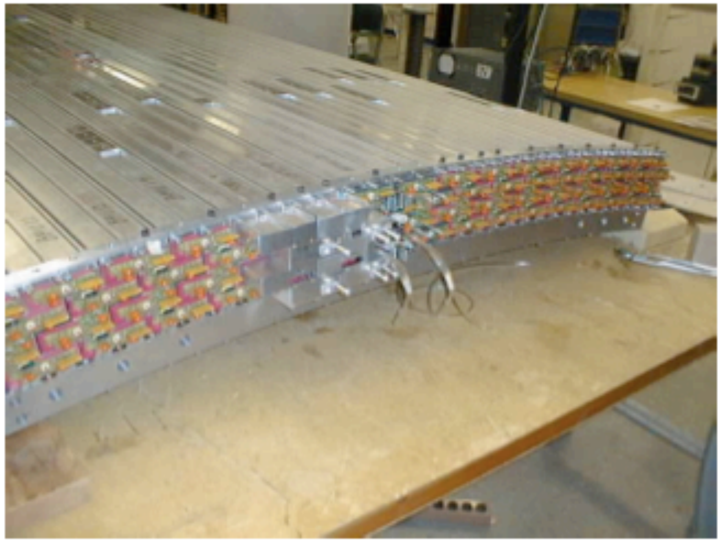

Driftchamber: Drift Velocity

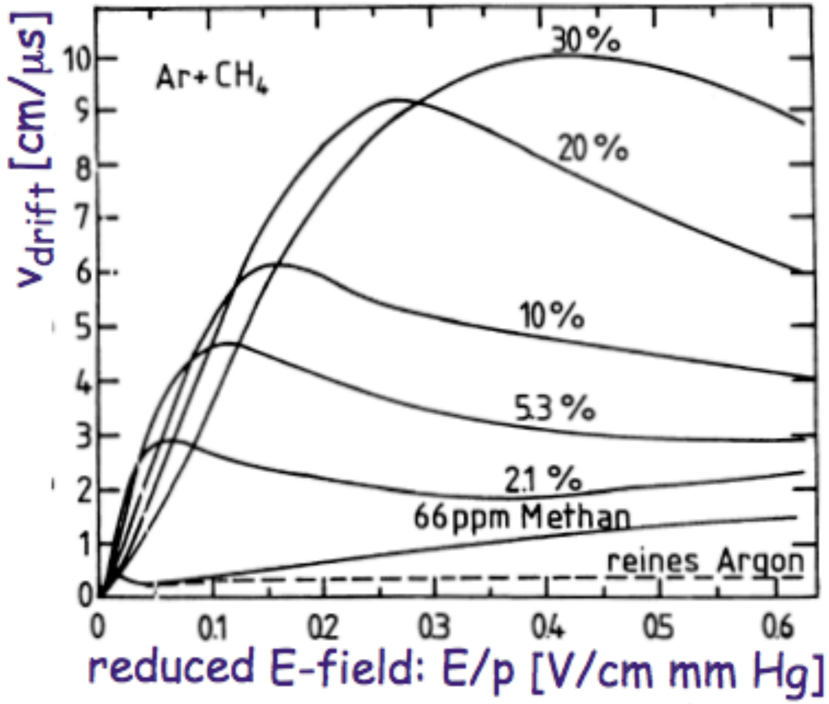

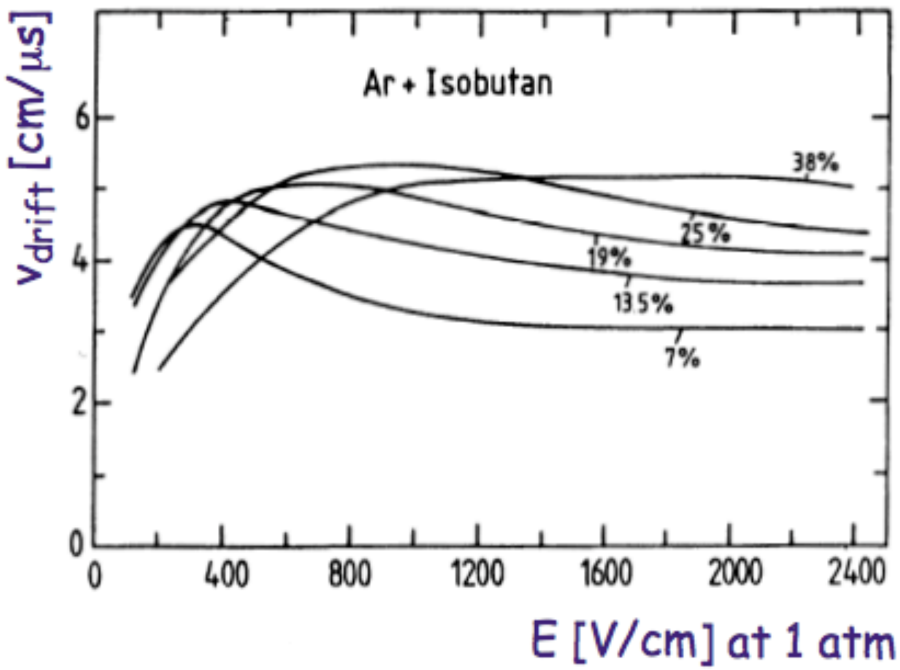

Some gas mixtures have a strong variation of drift velocity as function of E-field.

For stable operation it is useful to operate at maximum / plateau.

Typical drift velocities: 2-10 cm/μs = 20-100 ~m/ns.

Cylindrical Drift Chamber

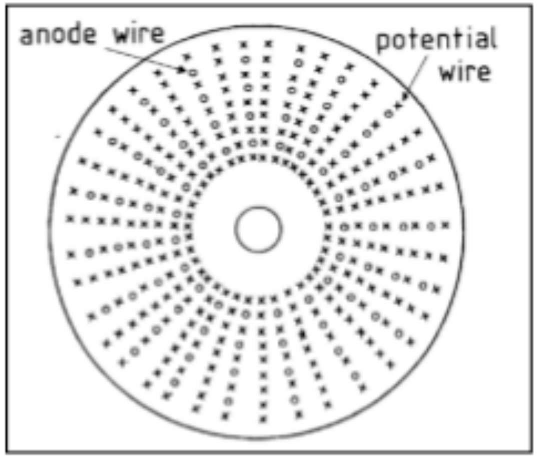

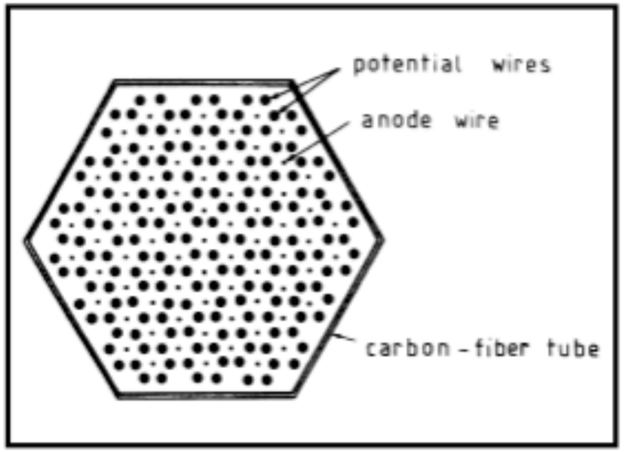

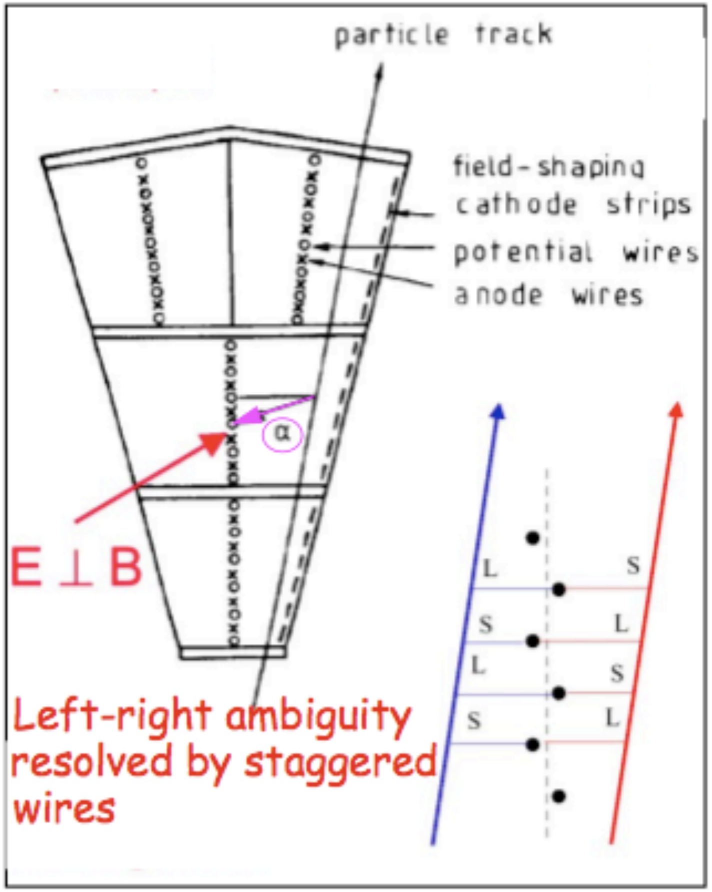

cell of a "jet"-driftchamber

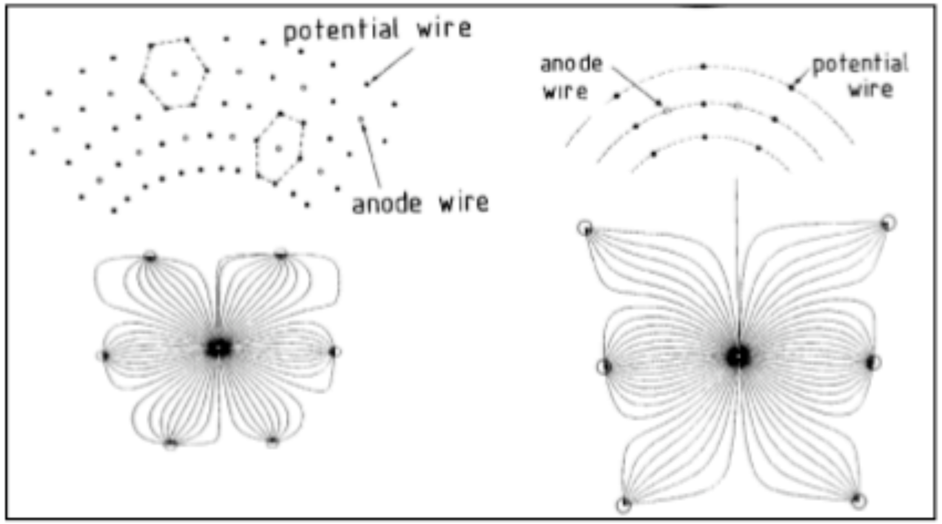

Cylindrical Drift Chamber

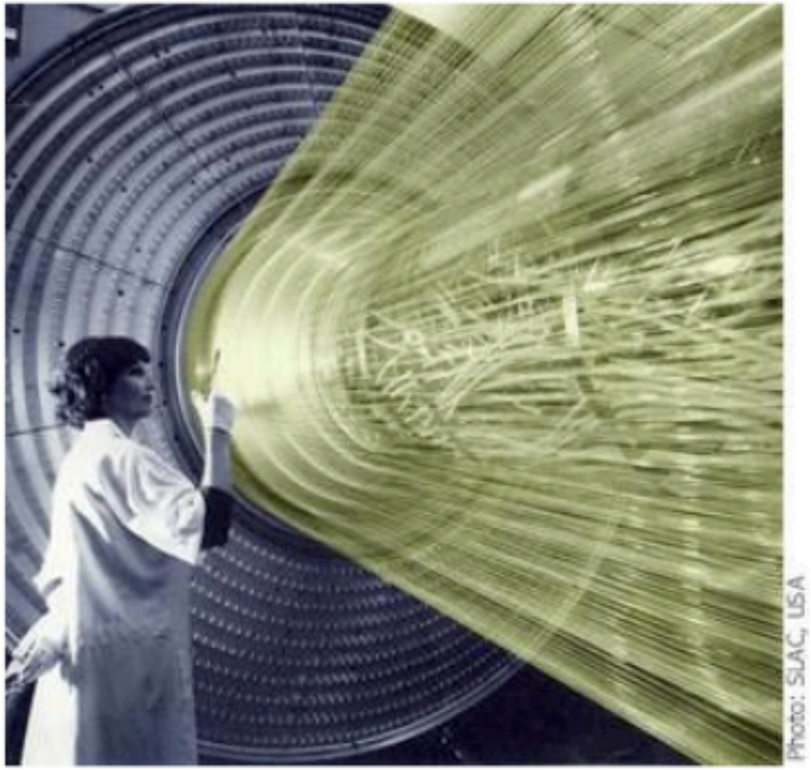

H1 Central Jet Chamber

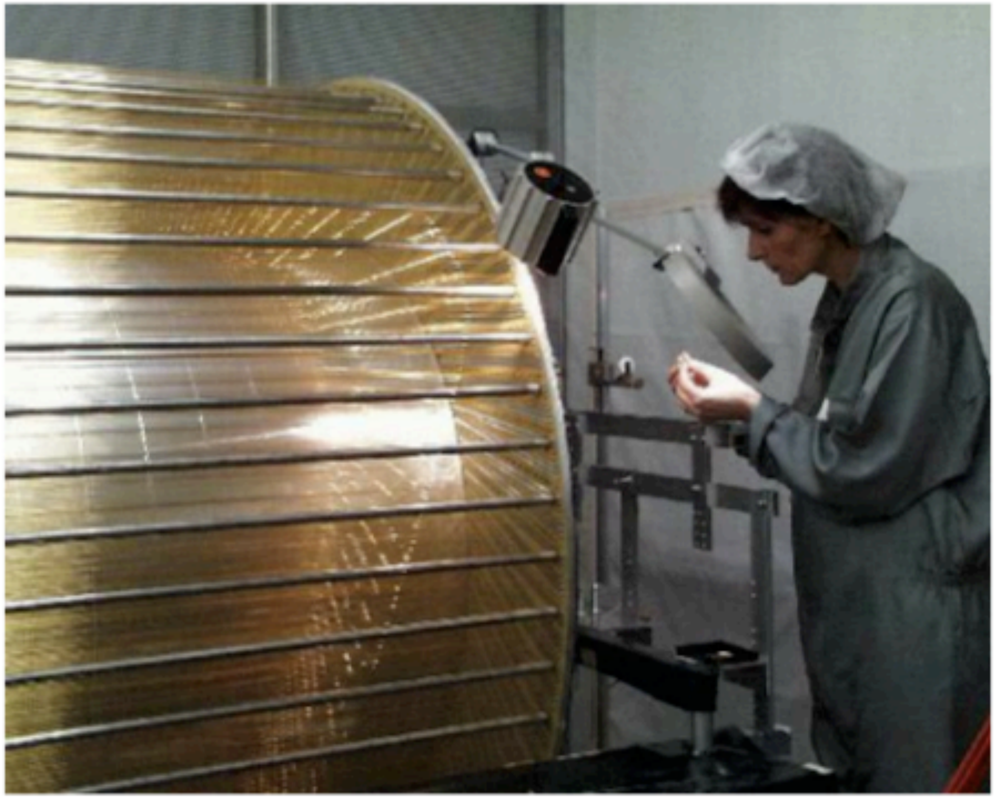

- ≈ 15000 wires
- total force from wire tension ≈ 6 tons

The ATLAS Muon Spectrometer

Monitored drift tubes	**MDT**
- Coverage	$\|\eta\| < 2.7$ (innermost layer: $\|\eta\| < 2.0$)
- Number of chambers	1088 (1150)
- Number of channels	339 000 (354 000)
- Function	Precision tracking
Cathode strip chambers	**CSC**
- Coverage	$2.0 < \|\eta\| < 2.7$
- Number of chambers	32
- Number of channels	31 000
- Function	Precision tracking
Resistive plate chambers	**RPC**
- Coverage	$\|\eta\| < 1.05$
- Number of chambers	544
- Number of channels	359 000
- Function	Triggering, second coordinate
Thin gap chambers	**TGC**
- Coverage	$1.05 < \|\eta\| < 2.7$ (2.4 for triggering)
- Number of chambers	3588
- Number of channels	318 000
- Function	Triggering, second coordinate

A complex system:

- 4 different technologies (MDT,CSC,RPC,TGC)
- Large area (10,000 m^2)
- Many channels (1M)

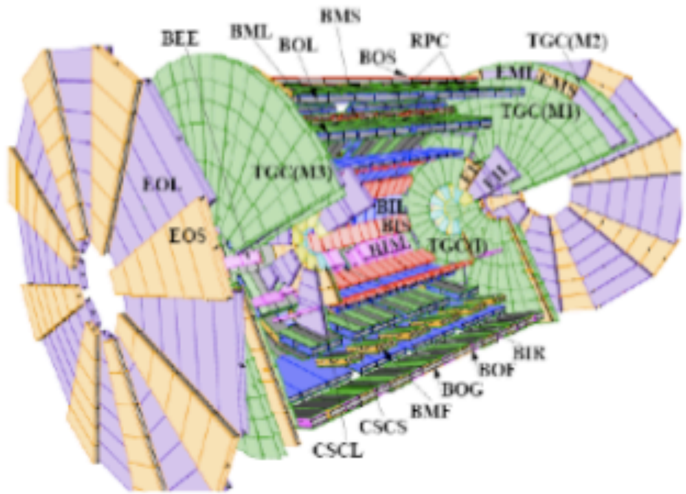

Time Projection Chamber (TPC)

from L. Ropelewski

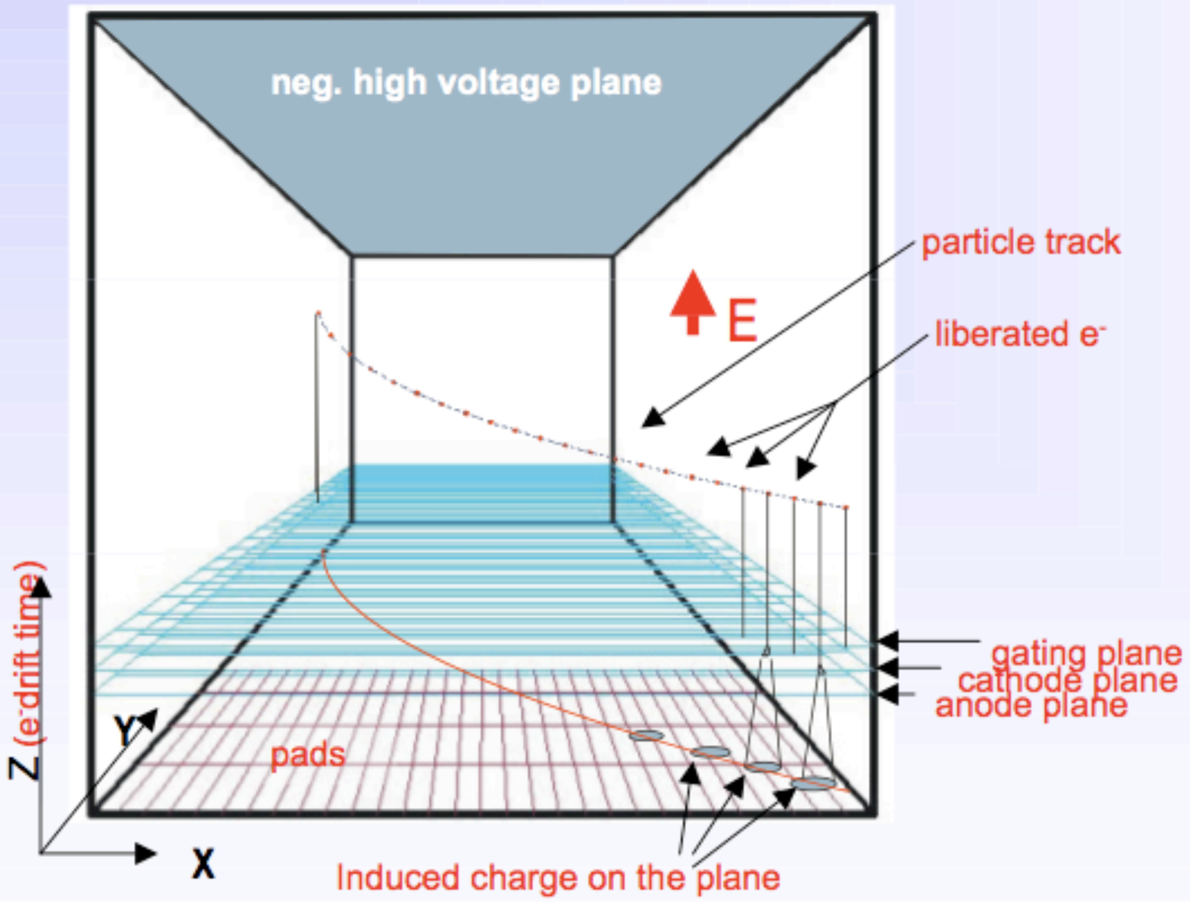

Time Projection Chamber

full 3D track reconstruction:

x-y from wires and segmented cathode of MWPC (or GEM)

z from drift time

- momentum resolution
  space resolution + B field (multiple scattering)
- energy resolution
  measure of primary ionization

TPC Time Projection Chamber

Developed by D. Nygren in the 70's.

Large gas volume with central electrode.

Drift distance of several meters.

Signal registered with MWPC, anode wires and cathode pads provide x,y ; drift time gives z.

Transverse diffusion reduced (electrons spiral around E-field, since E ll B, Lamor radius < 1 μm)

Very good 3D hit resolution and dE/dx.

Long drift times (≈ 40 μs), thus rate limitations and very good gas quality required.

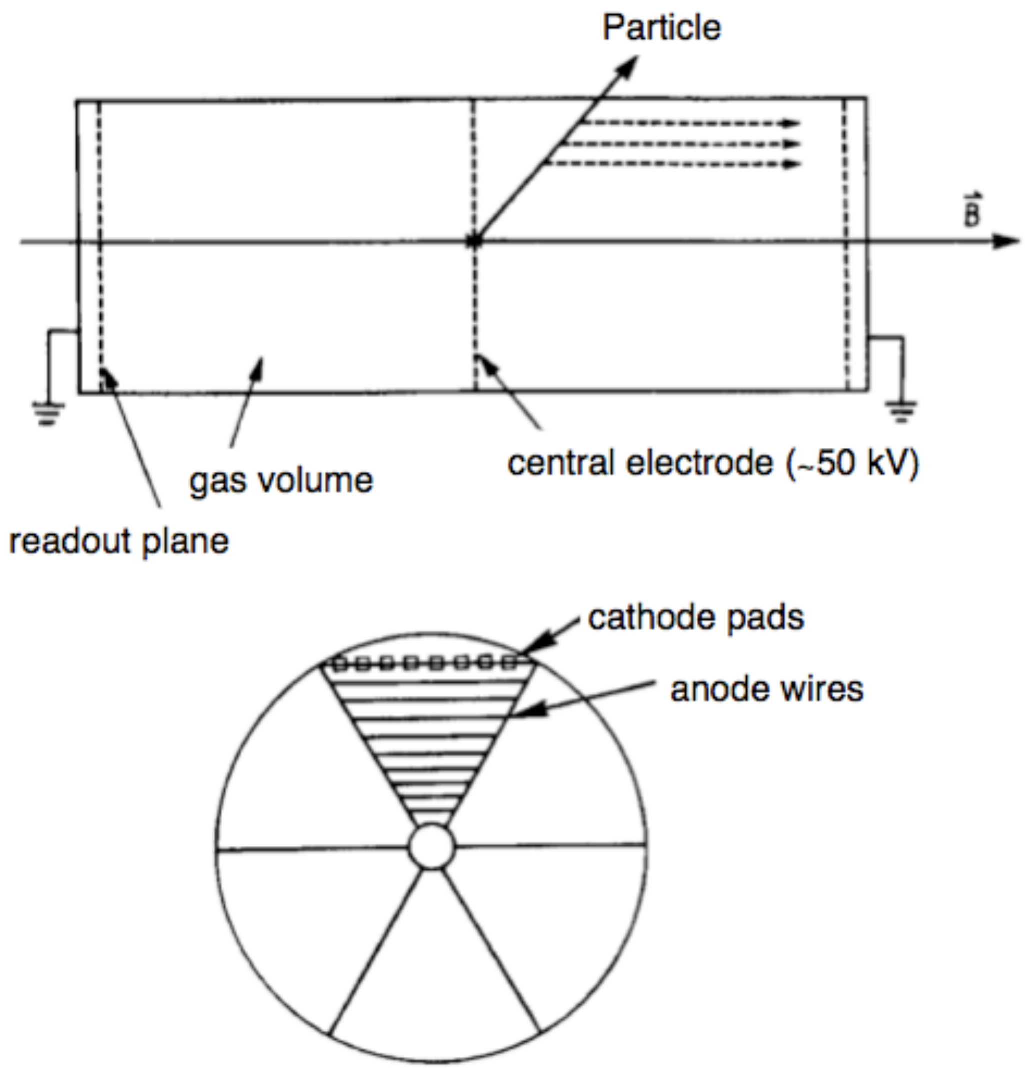

ALEPH TPC at LEP

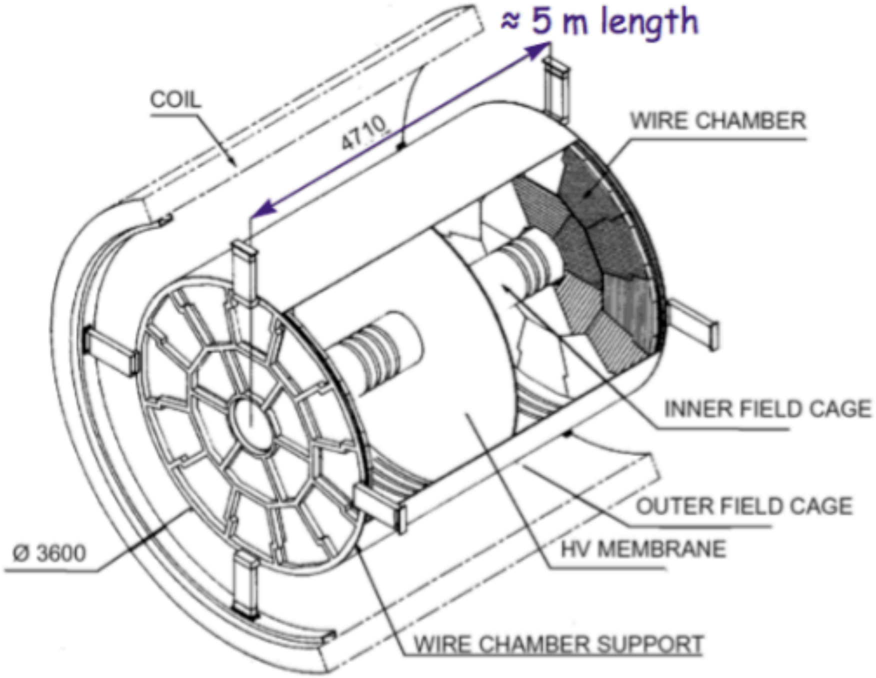

achieved resolutions:

$\sigma_{r\phi}$ = 170 μm

σ_z = 740 μm

r–φ projection

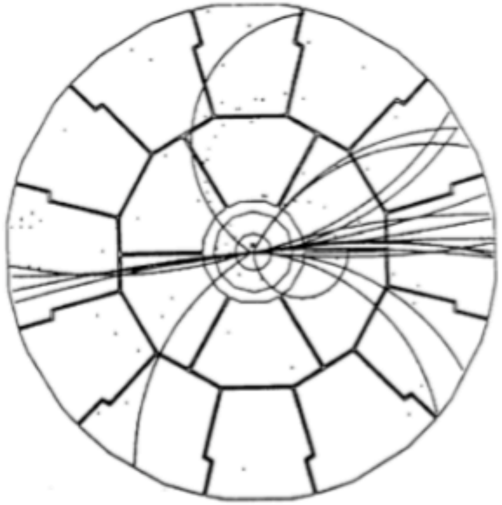

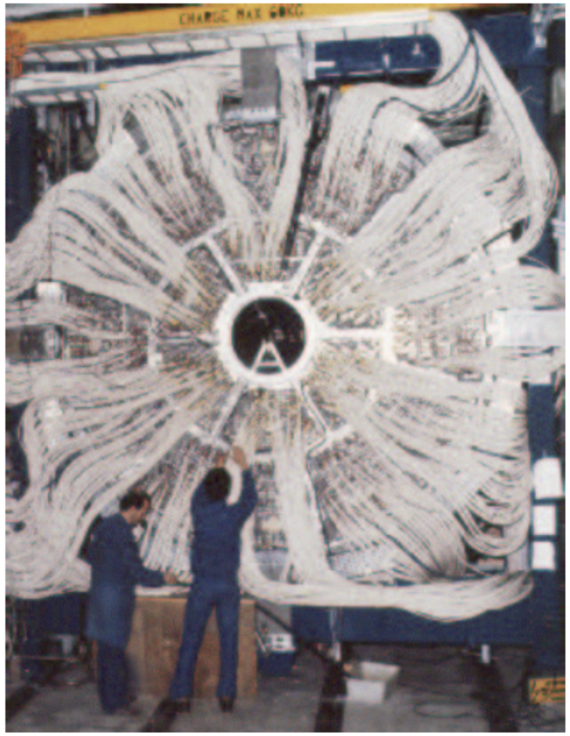

ALEPH TPC at LEP

Aleph Higgs Candidate Event: $e^+ e^- \to HZ \to b\bar{b} + jj$

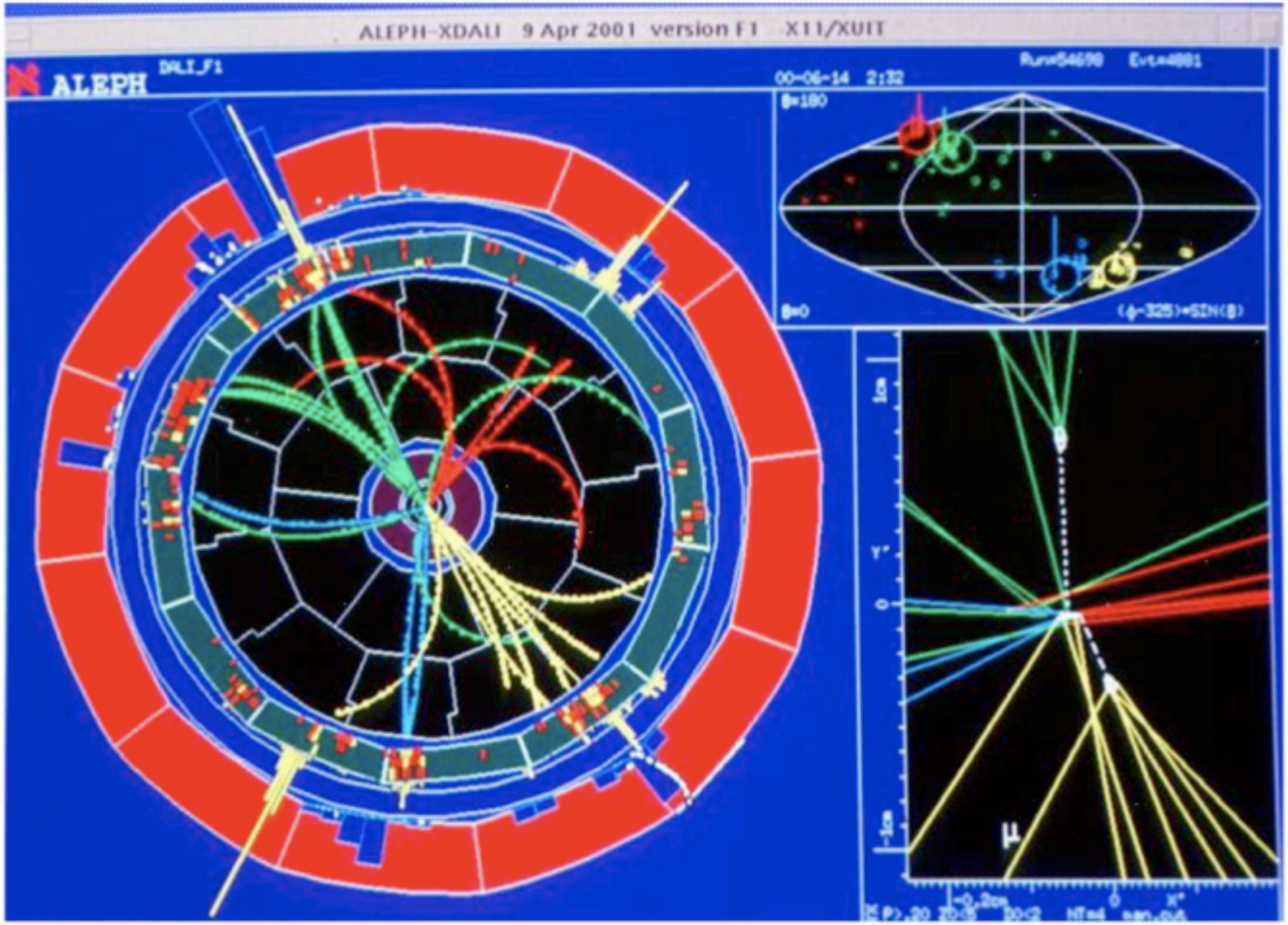

TPC for Heavy Ion Collisions

Au+ Au+ collision in the STAR Experiment/RHIC

Up to 2000 tracks

Pb+ Pb+ Kollision in the ALICE Experiment/LHC

Simulation for

Angle Θ=60 to 62°

Up to 40 000 tracks/collision

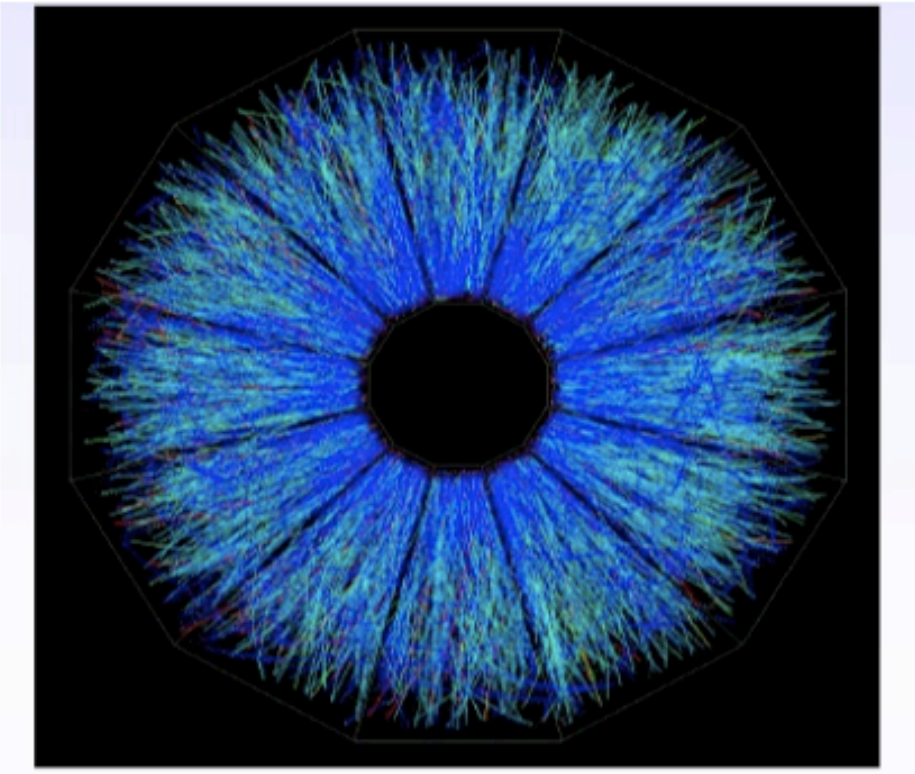

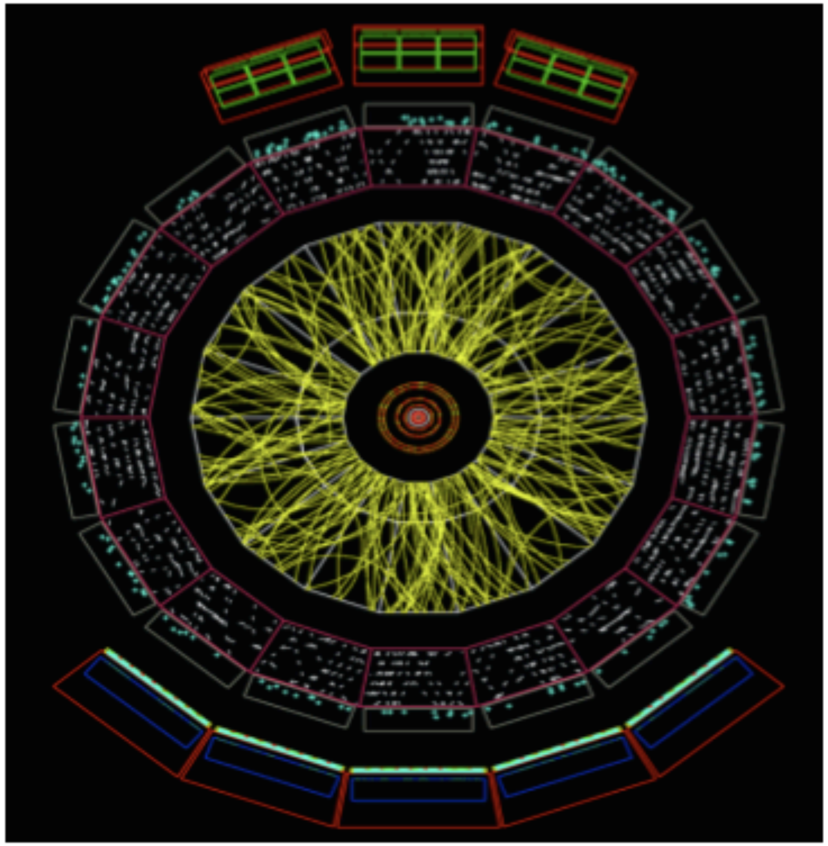

Micropattern Gas Chambers

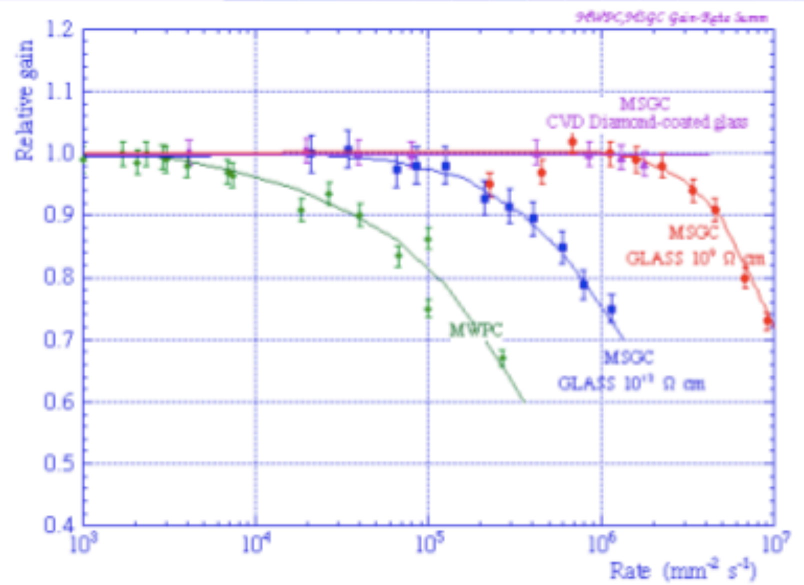

Advantages of gas detectors:

from L. Ropelewski

- low radiation length
- large areas at low price
- flexible geometry
- spatial, energy resolution …

Problem:

- rate capability limited by space charge defined by the time of evacuation of positive ions

scale factor

1

5

10

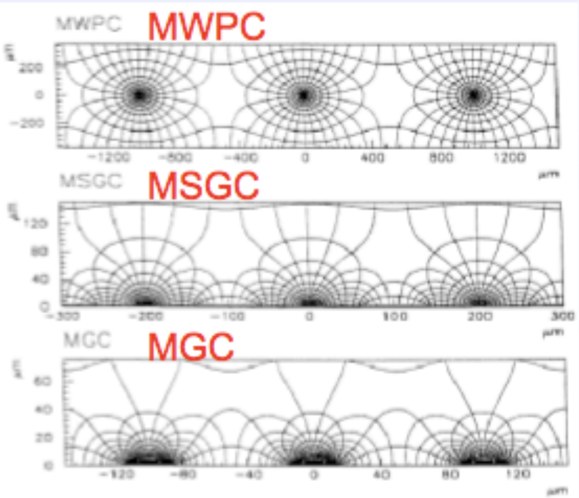

R. Bellazzini et al.

Solution:

- reduction of the size of the detecting cell (limitation of the length of the ion path) using chemical etching techniques developed for microelectronics and keeping at same time similar field shape.

Microstrip Gas Chamber

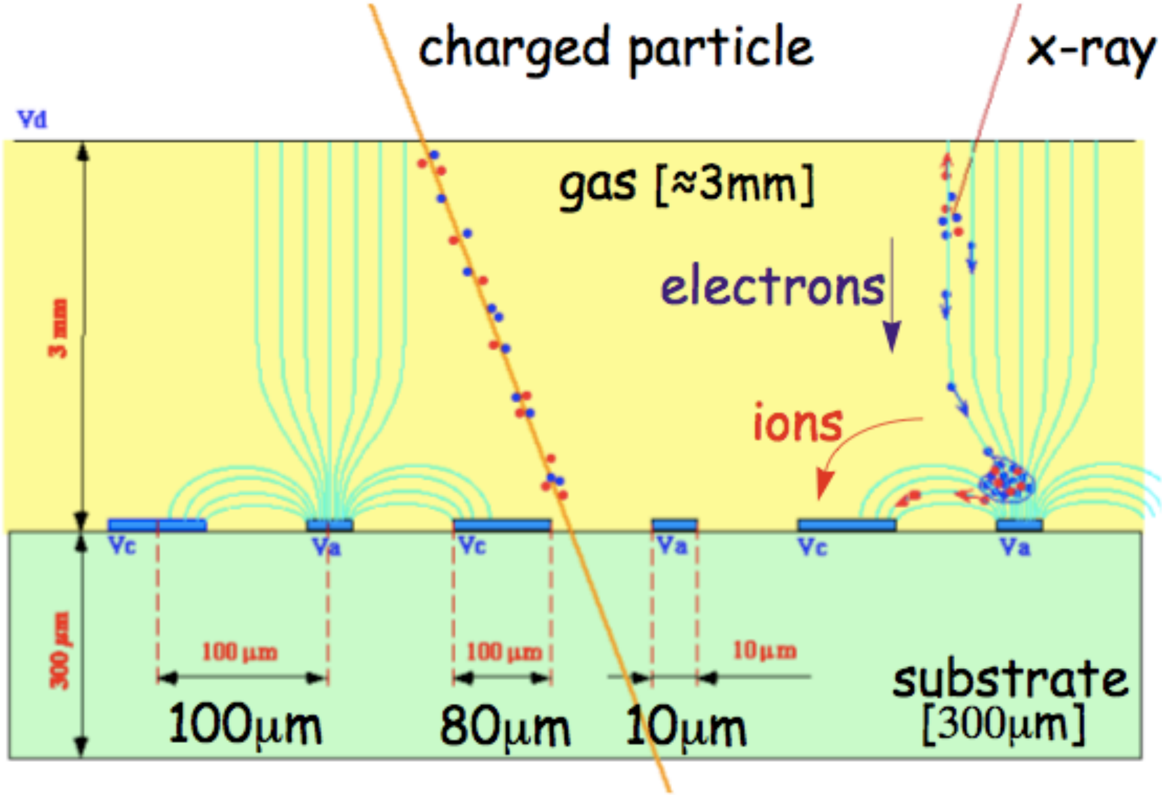

Advantages:

- Very precise and small anode/cathode structures can be produced with lithographical methods. Thus very good position resolution is possible.
- MSGC provide high mechanical stability
- small drift distance for ions, thus high rate capability.

Micromegas: Micromesh Gaseous Structure

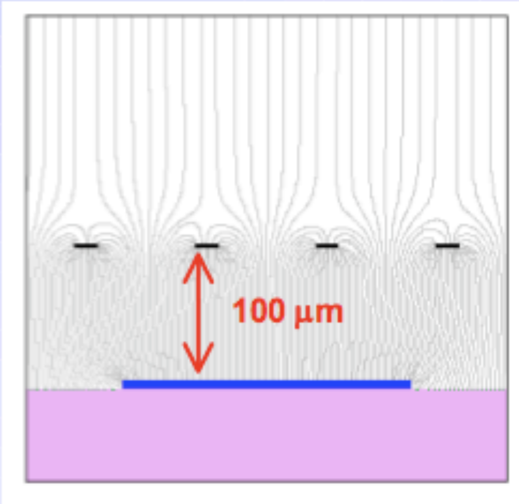

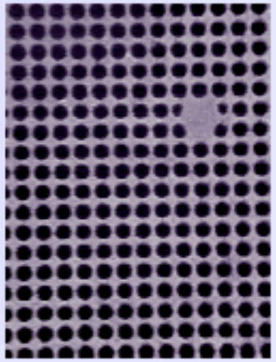

micromesh

Micromesh mounted above readout structure (typically strips).

E field similar to parallel plate detector.

E_a/E_i ~ 50 to secure electron transparency and positive ion flowback supression.

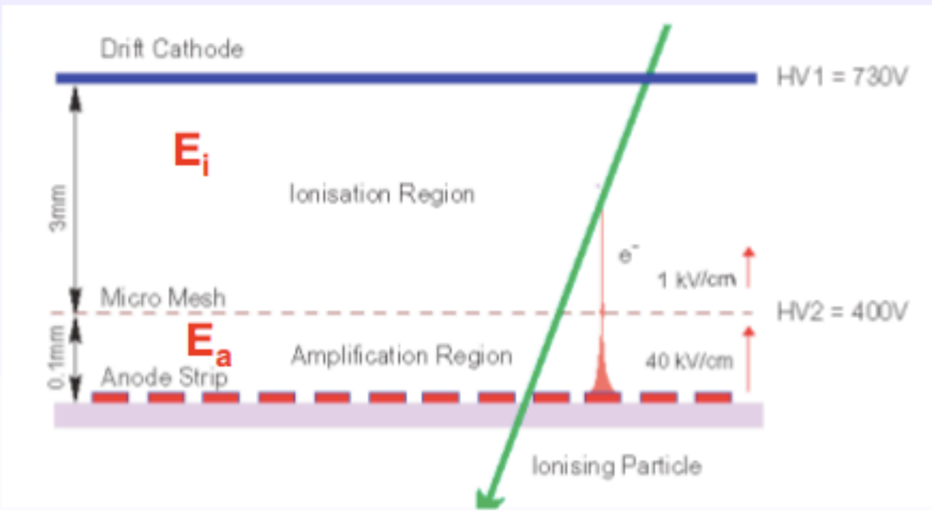

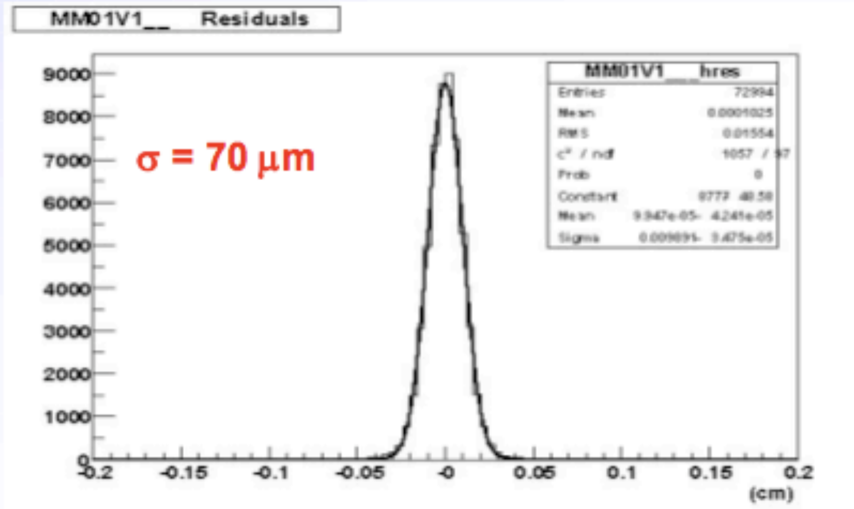

Space resolution

from L. Ropelewski

Gas Electron Multiplier

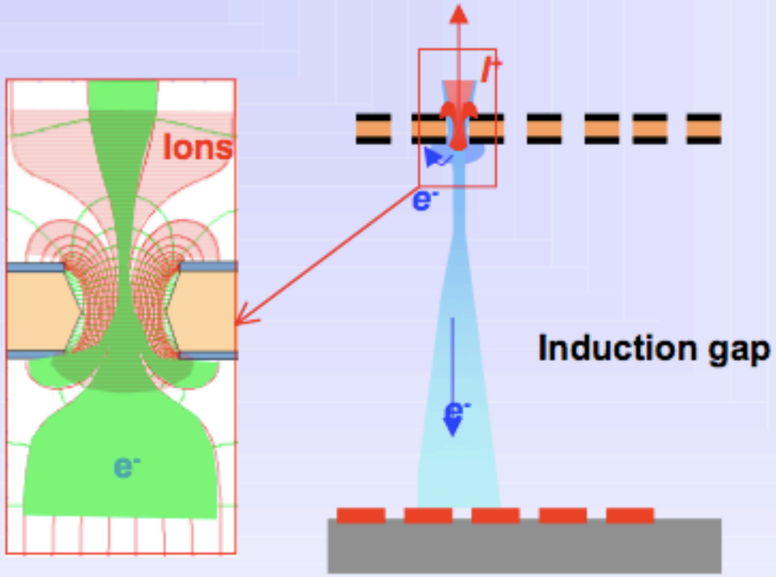

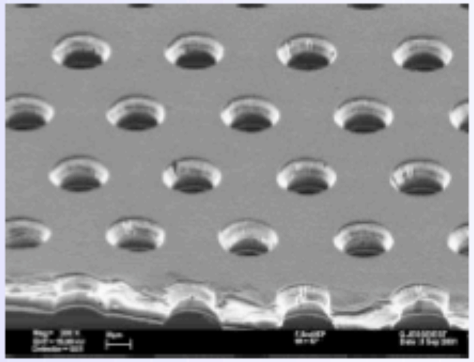

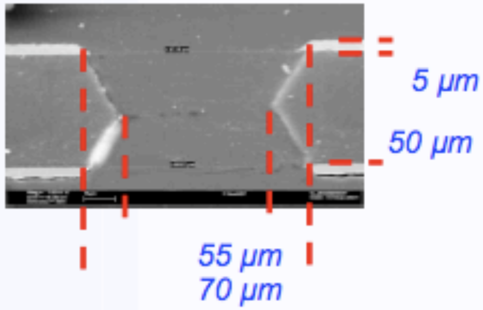

Thin, metal coated polyimide foil perforated with high density holes.

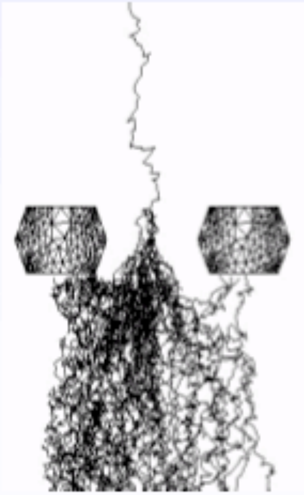

Electrons are collected on patterned readout board.
A fast signal can be detected on the lower GEM electrode for triggering or energy discrimination.
All readout electrodes are at ground potential.
Positive ions partially collected on the GEM electrodes.

from L. Ropelewski

GEM: Gas Electron Multiplier

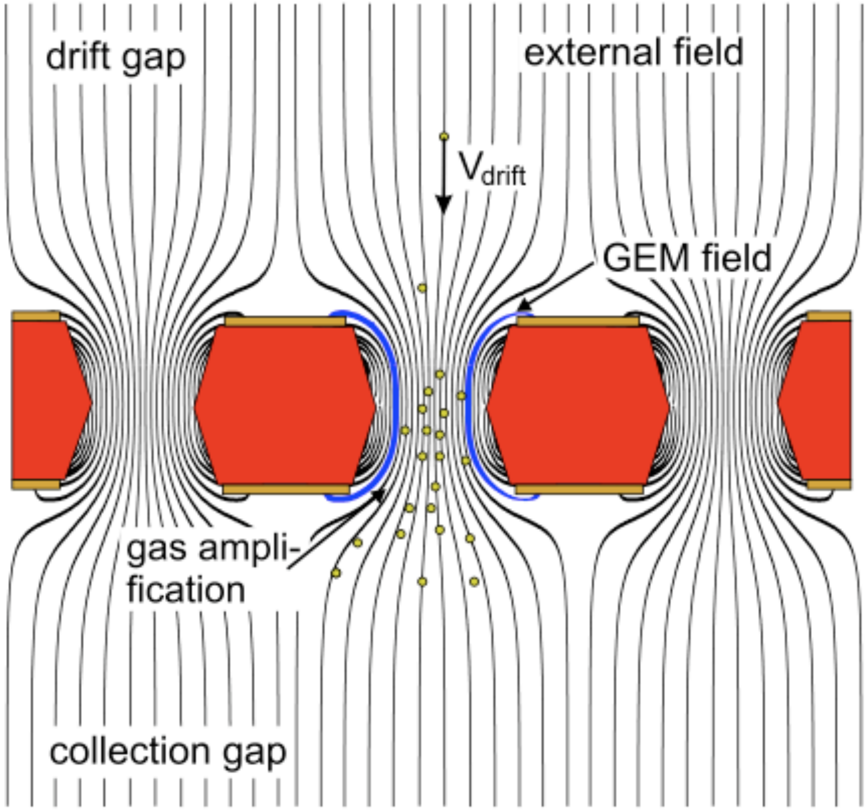

P. Cwetanski, thesis, Heidelberg

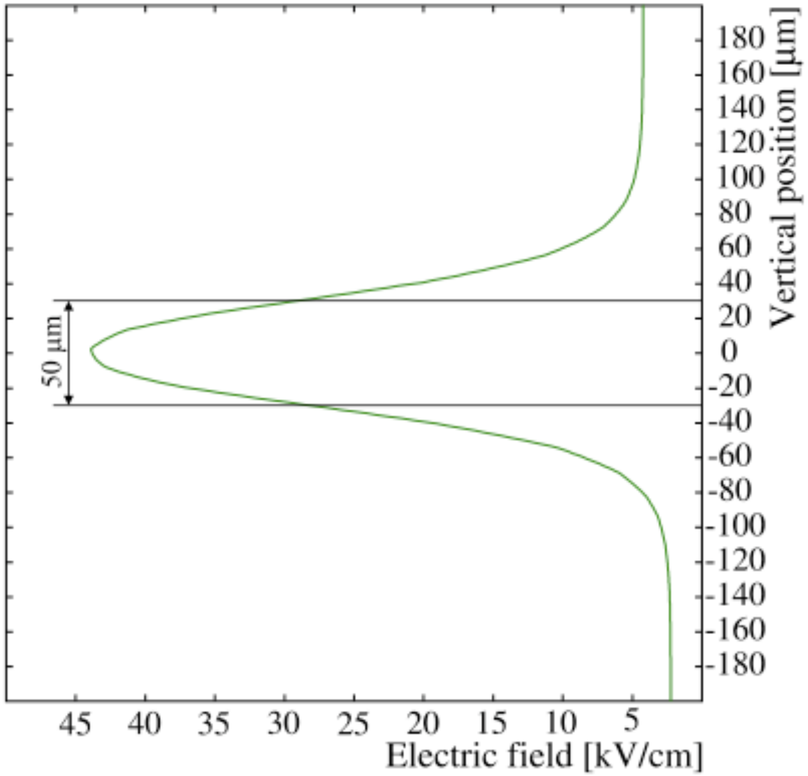

For a voltage between the GEM foils of 360 V the E-Field inside the gap reaches very high values, which cause gas amplification.

GEM Characteristics

- Rate capability ~ 1 MHz mm^{-2}
- Position accuracy (MIPs) σ ~ 60 μm
- Radiation tolerance > 100 mC mm^{-2}
  - corresponds to ~ 10^{14} MIPs cm^{-2}

Double-Gem

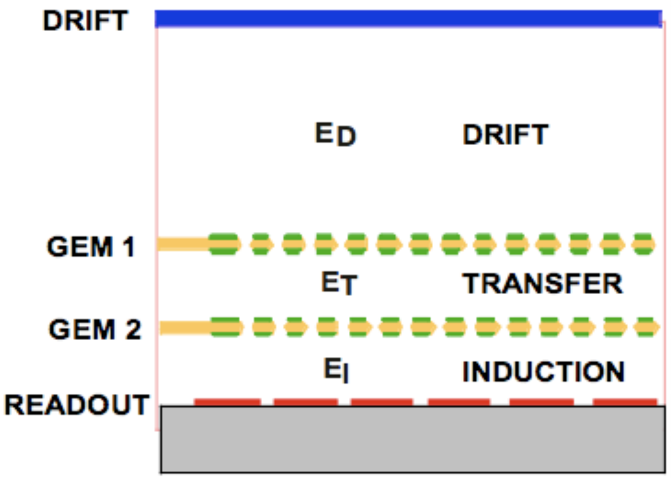

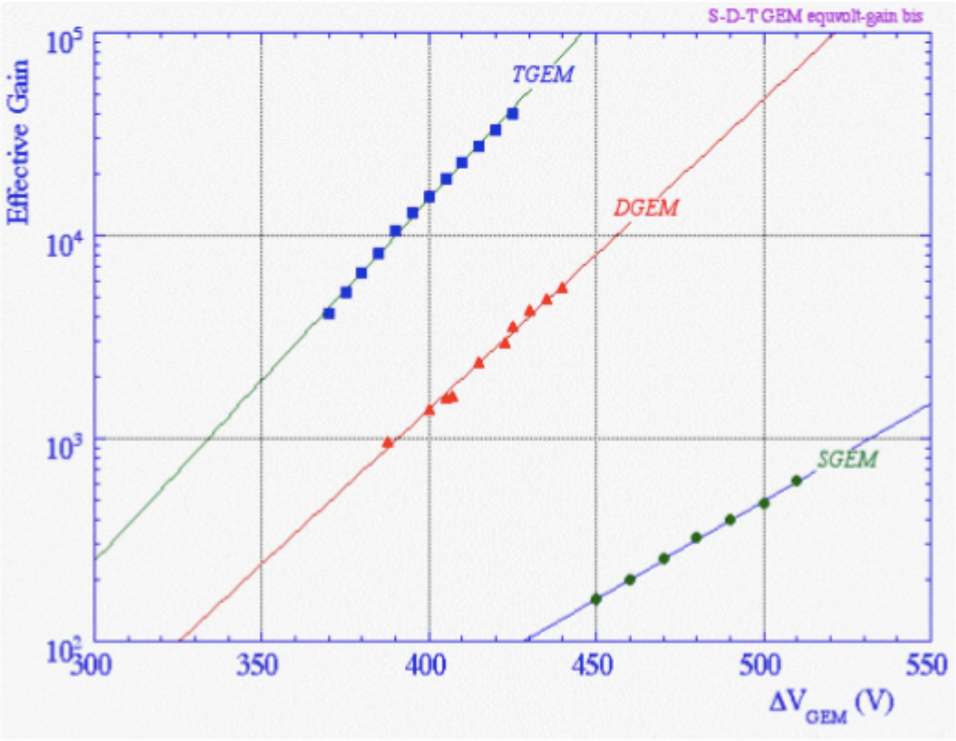

Semiconductor Detectors

Need for semi-conductor tracker

$$B_s^0 \rightarrow \psi'(\rightarrow \mu^+\mu^-)\phi(\rightarrow KK)$$

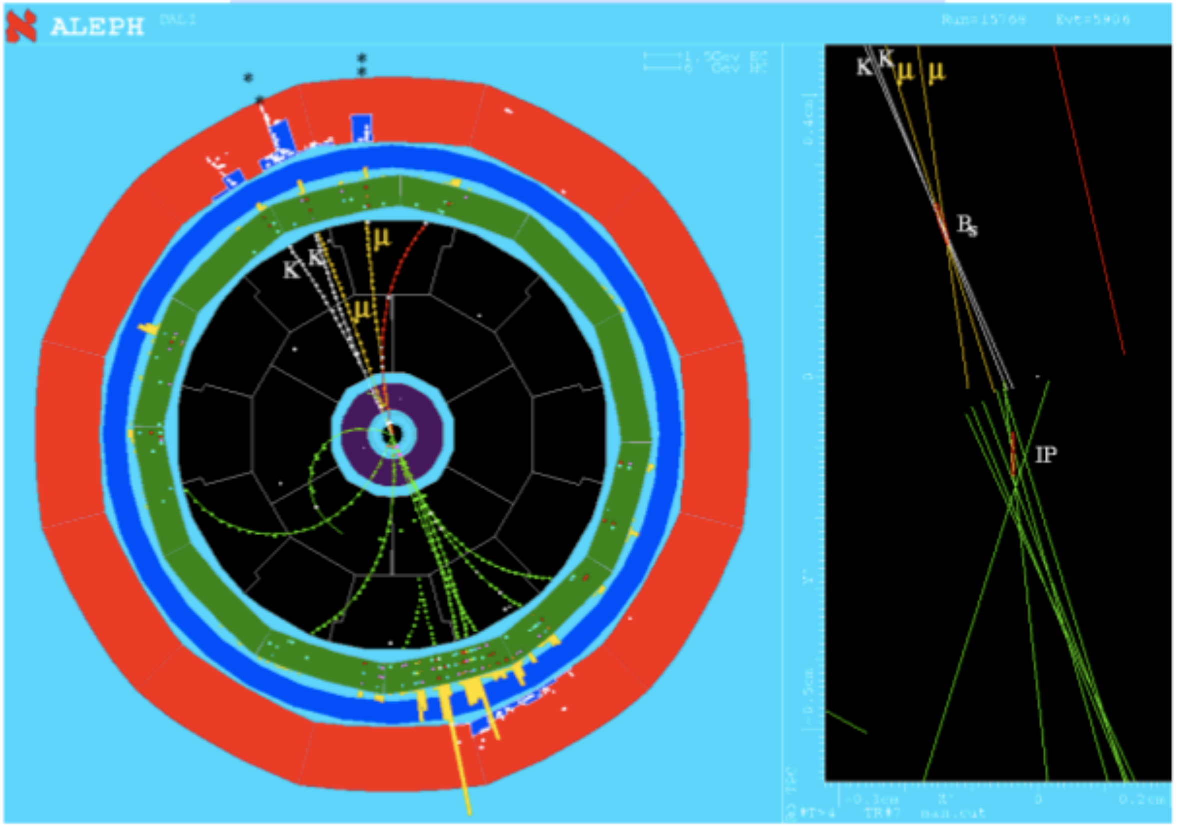

10 m　　0.5 mm

Aleph event:

Fully reconstructed B_s decay.

Track measurements with a precision of a few μm near the interaction point improve the momentum measurement and allow to determine the decay vertex, especially important for bottom hadrons.

Vertex Reconstruction

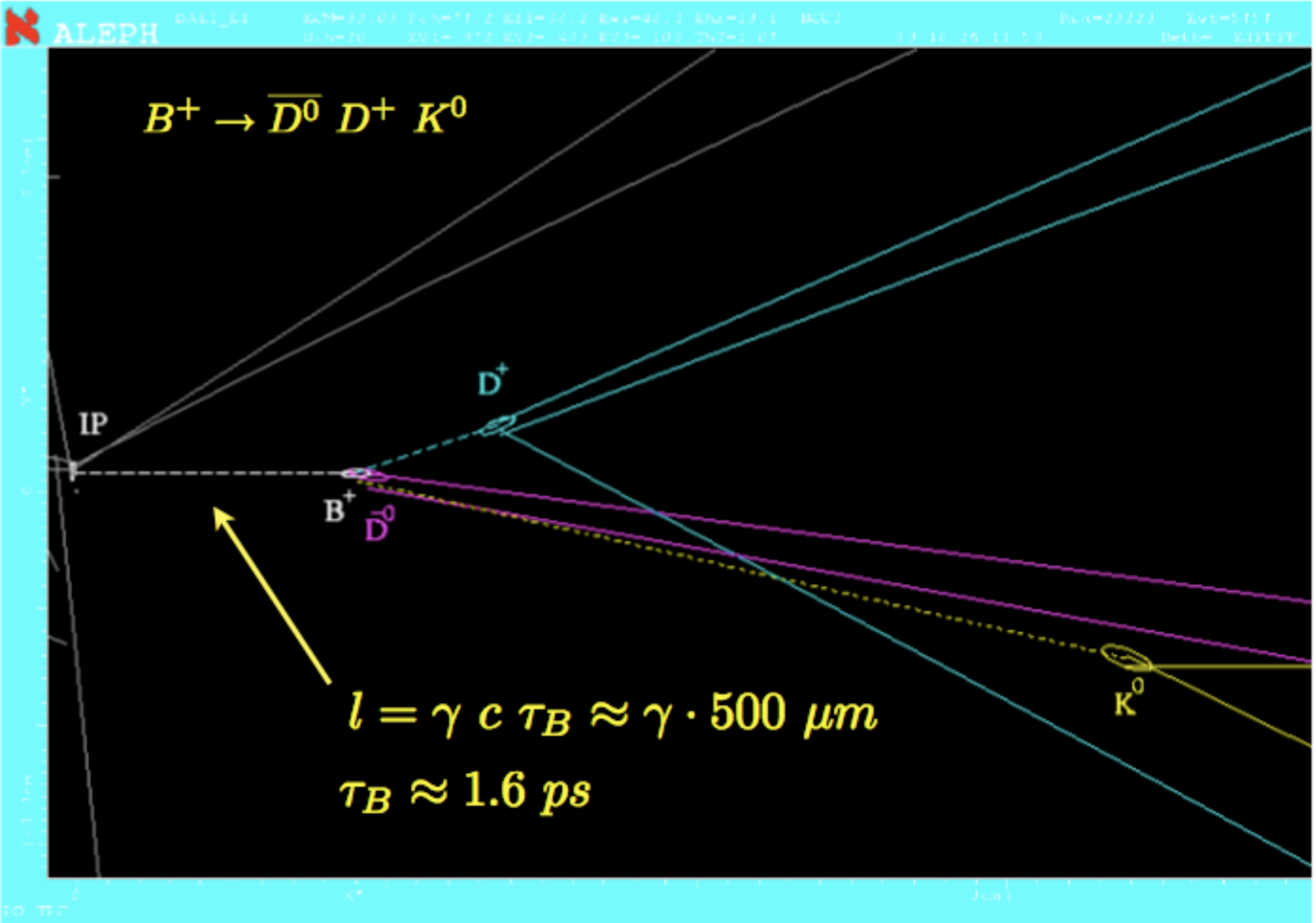

The life time of B-mesons can be measured from the decay length l, if the momentum of the B-meson (γ-factor) is measured as well.

Vertexing at the LHC

pp → ttH (m=120 GeV)
H → bb
tt → W(lvl)b W(qq)b

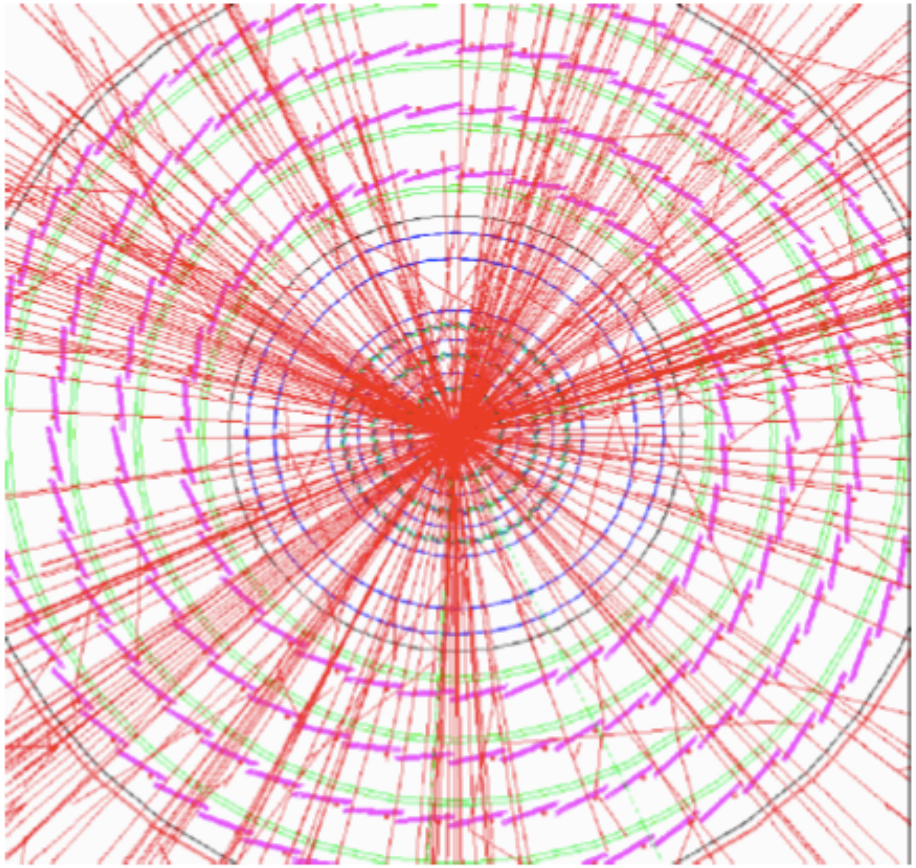

~ 1200 tracks/BX

high track density
in particular in jets

3D hit information
mandatory

↓

pixels

Solid State Tracking Detector - Silicon

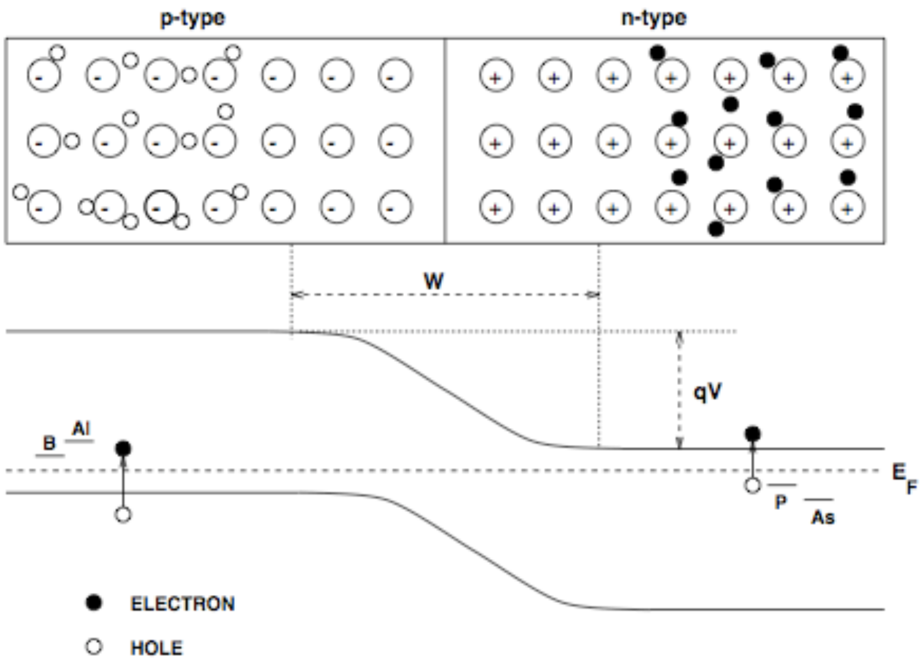

p-n junction (diode).

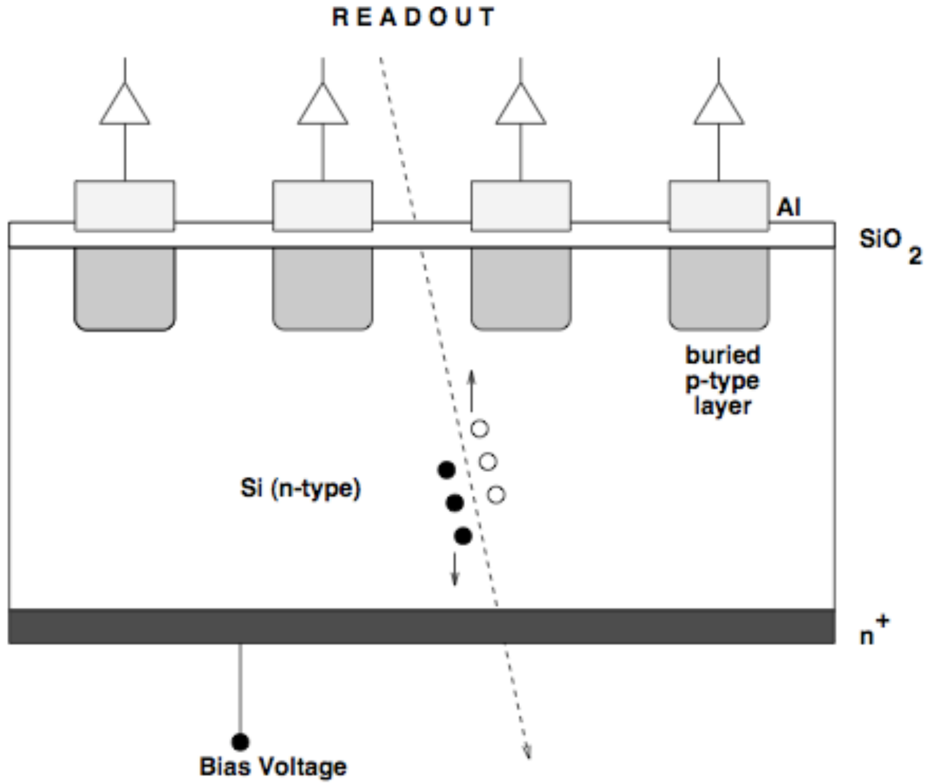

Silicon:

$dE/dx \approx 3.8\,\mathrm{MeV/cm}$, Band Gap 1.1 eV

3.6 eV to produce one electron-hole pair

Typical thickness: 300 μm

Strip Distance: $\geq 10\ \mu$m

Doped Semiconductor Detectors

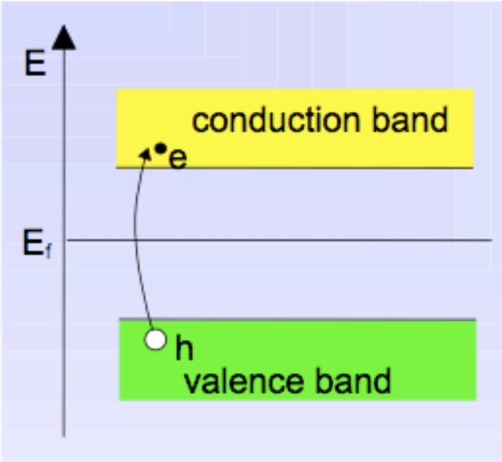

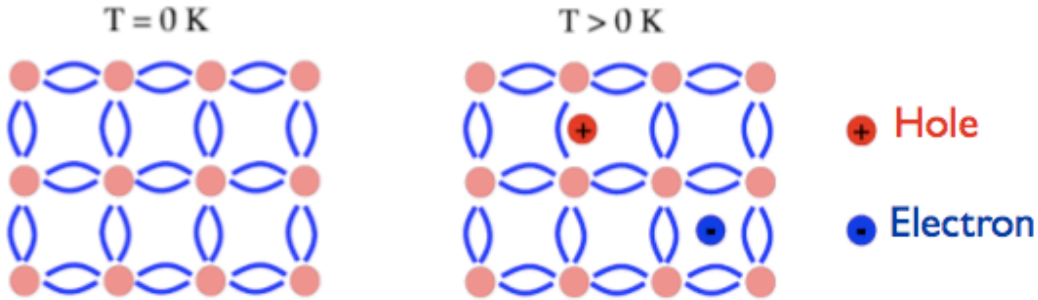

Silicon and germanium have 4 valence electrons, thus four covalent bounds. Thermal excitation excites electrons to the conduction band, which creates holes in the valence band.

Intrinsic electron(hole) concentration: $n_i = A\,T^{3/2}\ \exp(-\,E_g/2kT)$

(Si: Energy gap E_g = 1.12 eV, Ge: E_g=0.66 eV, T=20 ^{0}C $\Rightarrow$ kT=1/40 eV)

Typical values at T = 300 K (compare to silicon concentration of 5 x 10^{22} cm^{-3})

Si: n_i = 1.5 x 10^{10} cm^{-3}

Ge: n_i = 2.5 x 10^{13} cm^{-3}

Silicon Strip Detector

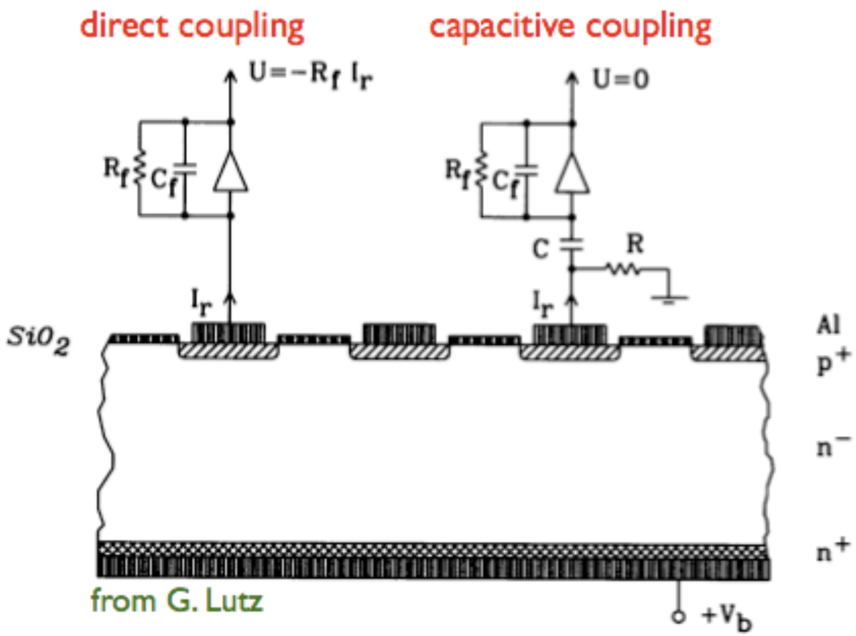

from G. Lutz

Direct coupling: reverse current I_r is absorbed by electronics.

Capacitive coupling: AC part goes to amplifier,
DC part goes through bias resistor R.

Typical detector thickness: 300 μm (150μm - 500 μm)

Typical strip separation, pitch p: 20 μm - 150 μm

Position resolution: $\sigma = p / \sqrt{12} \simeq 14$ μm (p=50 μm)

- Bias resistor produced by deposition of polysilicon.
- Capacitors produced via metal readout lines over implants (S_iO_2 isolation).

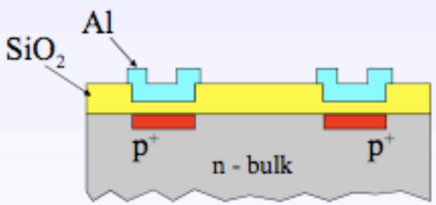

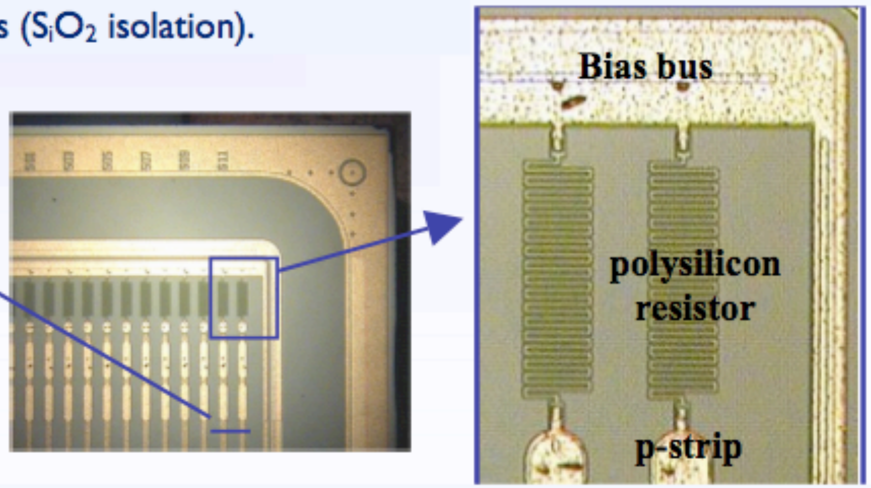

Several different methods are used to readout strips and to provide bias voltage. They are implemented in the manufacturing process.

Measured Signal

- Collected Charge for a Minimum Ionizing Particle (MIP)

- **Mean energy loss**
  dE/dx (Si) = 3.88 MeV/cm
  ⇒ 116 keV for 300μm thickness

- **Most probable energy loss**
  ≈ 0.7 ×mean
  ⇒ 81 keV

- **3.6 eV to create an e-h pair**
  ⇒ 72 e-h / μm (mean)
  ⇒ 108 e-h / μm (most probable)

- **Most probable charge** (300 μm)

  ≈ 22500 e ≈ 3.6 fC

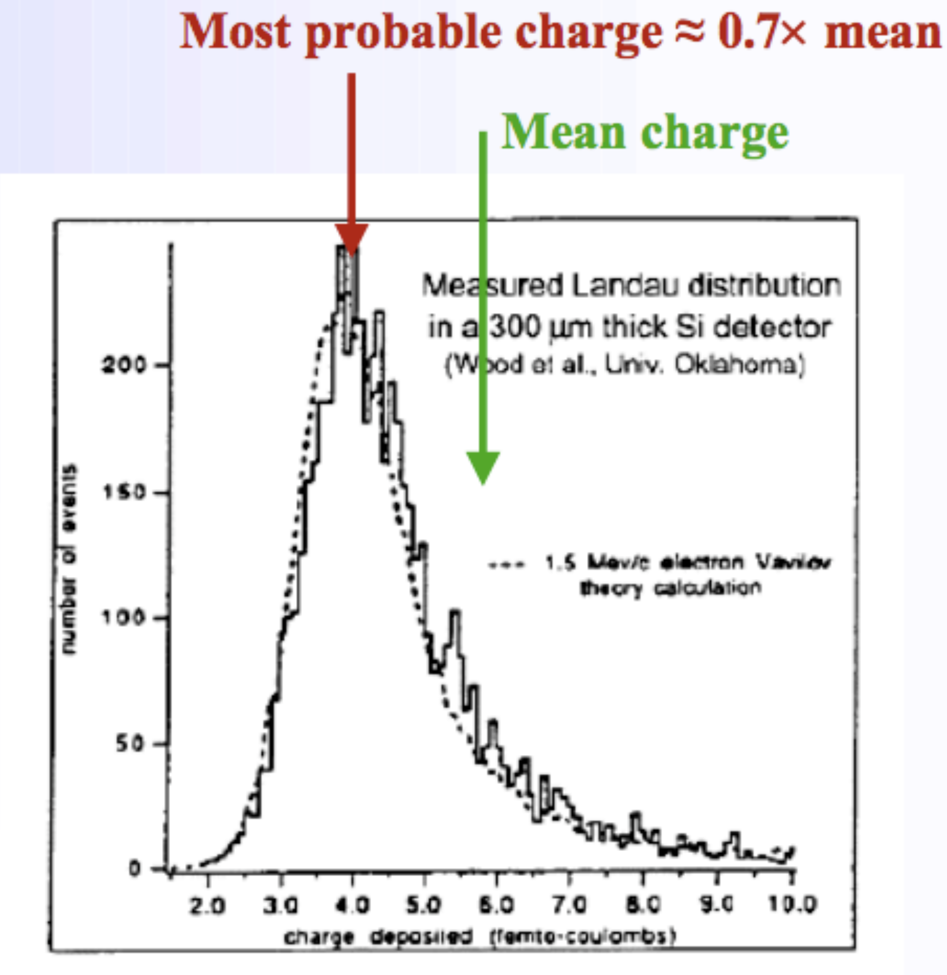

from M. Moll

Charge Collection and Diffusion

Charge collection time:

Drift velocity of charge carriers $v \simeq \mu E$ and drift time $t_d = d/v = d/\mu E$.

Typical values: d=300 μm, E=2.5 kV/cm (μ_e=1350 cm²/Vs and μ_h=450 cm²/Vs).

Drift times: $t_d(e)$ = 9 ns, $t_d(h)$ = 27 ns

Diffusion:

Diffusion of charge cloud caused by scattering of charge carriers. Width of distribution increases with drift time t_d. Using the diffusion constant $D = \mu kT/e$ one finds:

$$\sigma = \sqrt{2Dt_d} = \sqrt{\frac{2dkT}{eE}}$$

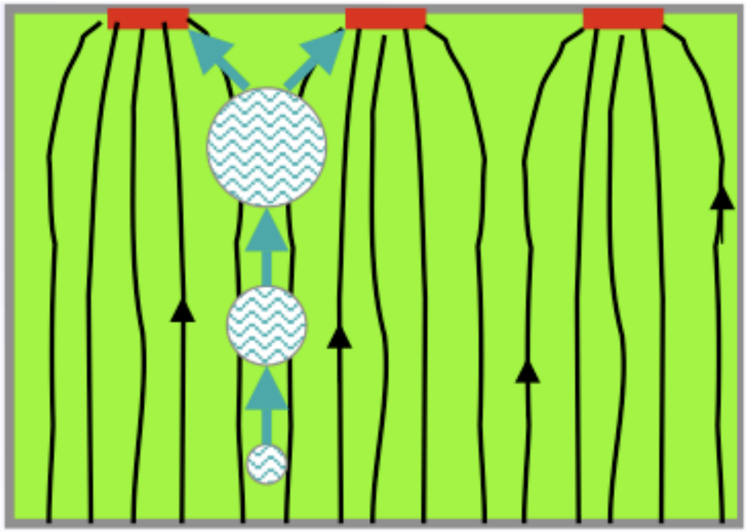

from M. Moll

Note that diffusion is the same for electrons and holes, since the mobility drops out.

Typical charge width: 8-10 μm in 300 μm thick silicon. Width of charge cloud could be exploited to obtain better position resolution due to charge sharing between strips (charge centroid finding).

Lorentz Angle in B-field

N. Wermes

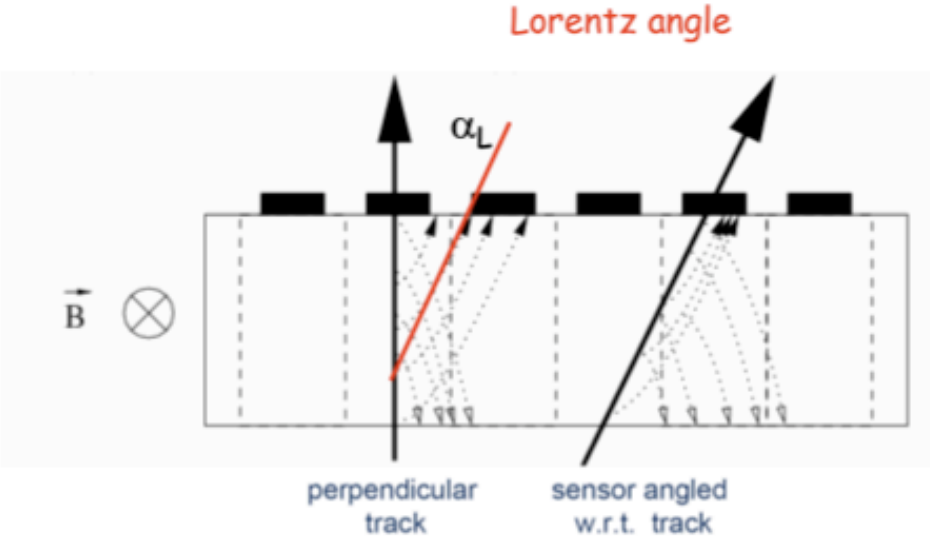

$$\tan \alpha_L = \mu_{Hall} B_\perp$$

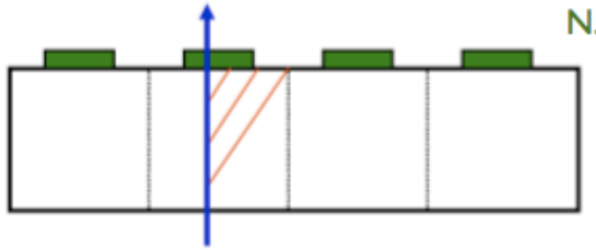

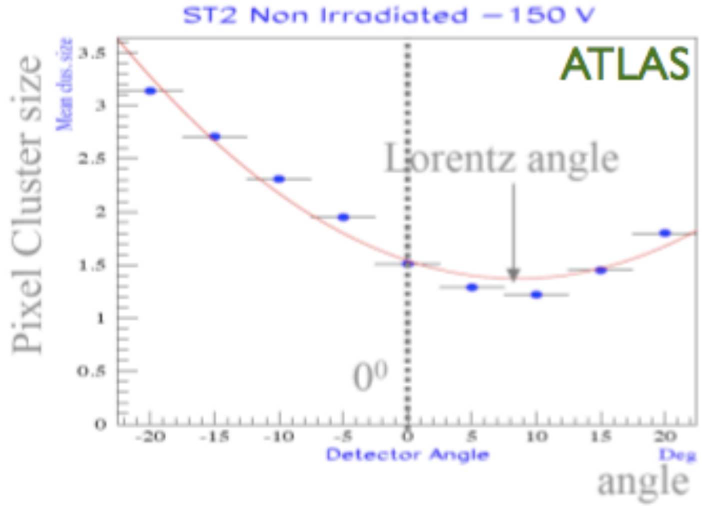

Measurement of Lorentz angle:
Number of strip (or pixel) hits is minimum, if incident angle of beam is equal to Lorentz angle.
Silicon detectors are built at a tilt angle to compensate for the Lorentz angle.

Effective incident angle = tilt angle + Lorentz angle

Detector Modules: ATLAS

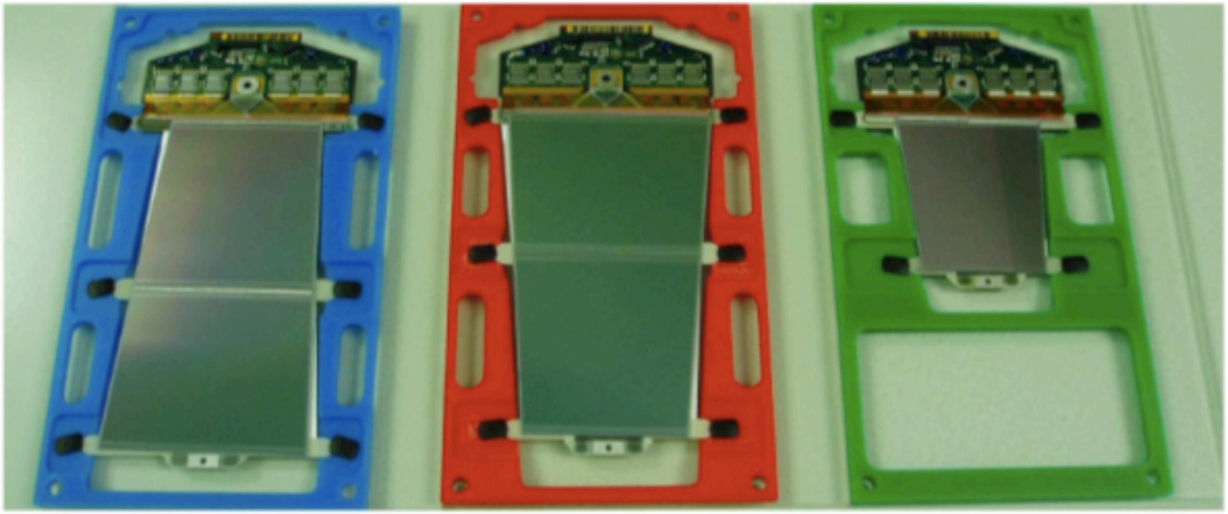

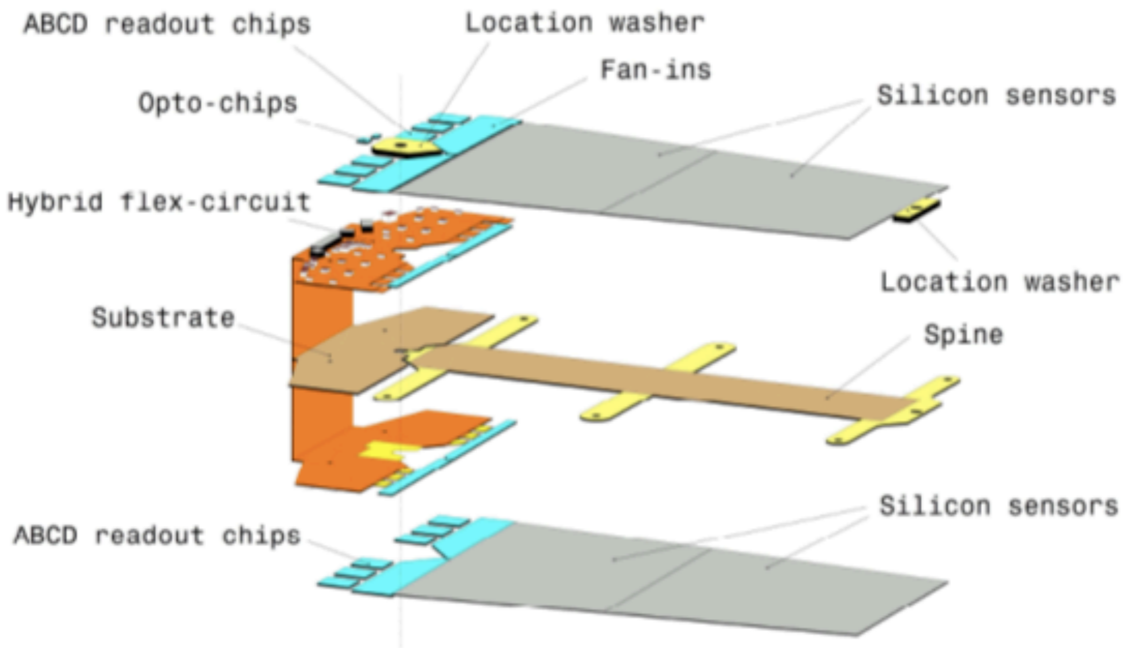

ATLAS Silicon central tracker SCT

Endcap:
1976 modules with 2 sensors glued back to back on spine.

Rotation by 20 mrad (Rφ resolution)

Spine conducts heat.

Alignment position of sensors ≈2 μm.

Strip pitch 80 μm, width 12 μm.

Resolution 16 μm in R-φ.

Operation temperature -7 °C.

99.8% of strips are working.

Other Silicon Detectors

- Double Sided Strip Detectors
  - Has strip structure also on back side, under 90°
  - Still no real 3d information
  - used to minimize material (multiple scattering)
  - more difficult to operate (noise)

- Silicon Drift
  - Same idea as (wire) drift chamber: Use time information
  - drift over several cm achieved (example: ALICE prototype)

- Silicon Pixel Detectors
  - No strips, but (usually rectangular) pixels
  - bonding for electronics very complicated, but doable (example: BTeV prototype)
  - give real 3d information
  - Usable for trigger

Hybrid Pixels

- **HAPS – Hybrid Active Pixel Sensors**
  - segment silicon to diode matrix with high granularity (⇒ true 2D, no reconstruction ambiguity)
  - readout electronic with same geometry (every cell connected to its own processing electronics)
  - connection by “bump bonding”
  - requires sophisticated readout architecture
  - Hybrid pixel detectors will be used in LHC experiments: ATLAS, ALICE, CMS and LHCb

Solder Bump: Pb-Sn

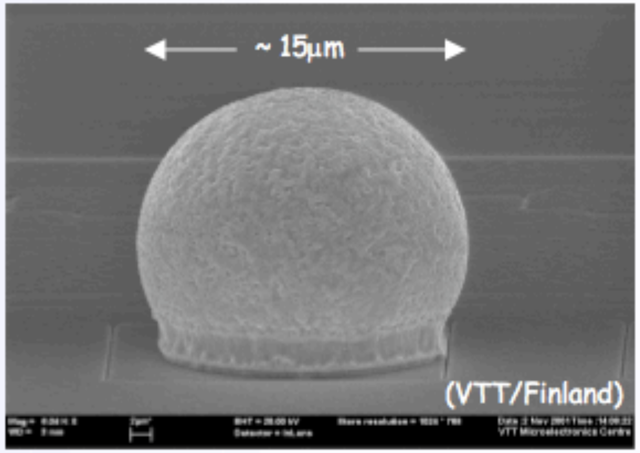

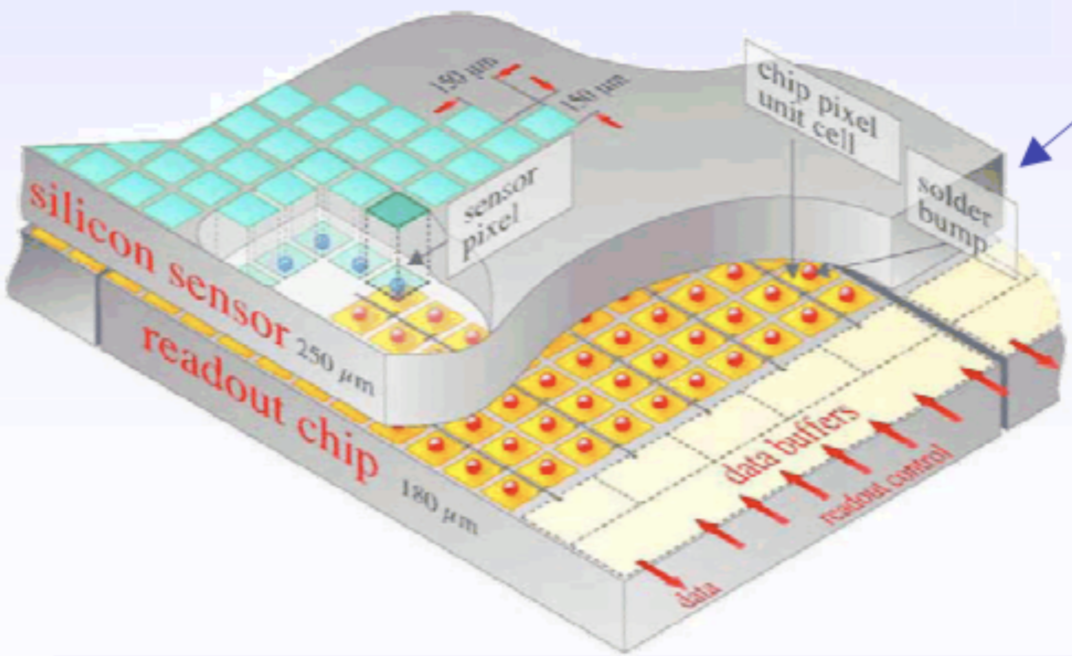

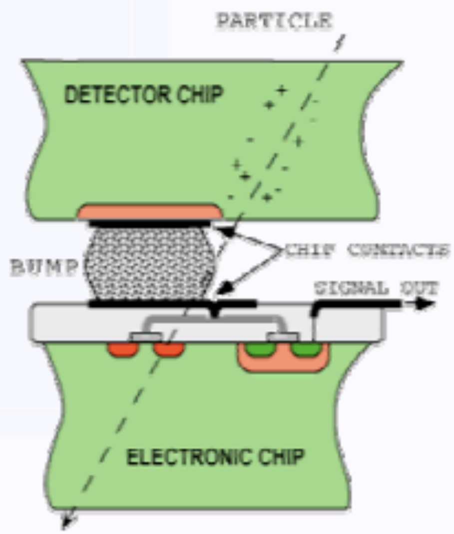

Flip-chip technique

from M. Moll

New Vertex Detector for CDF (or D0?). 1 Million strips

END

Radiation Damage

Example: ATLAS

- Fluences per year at full Luminosity

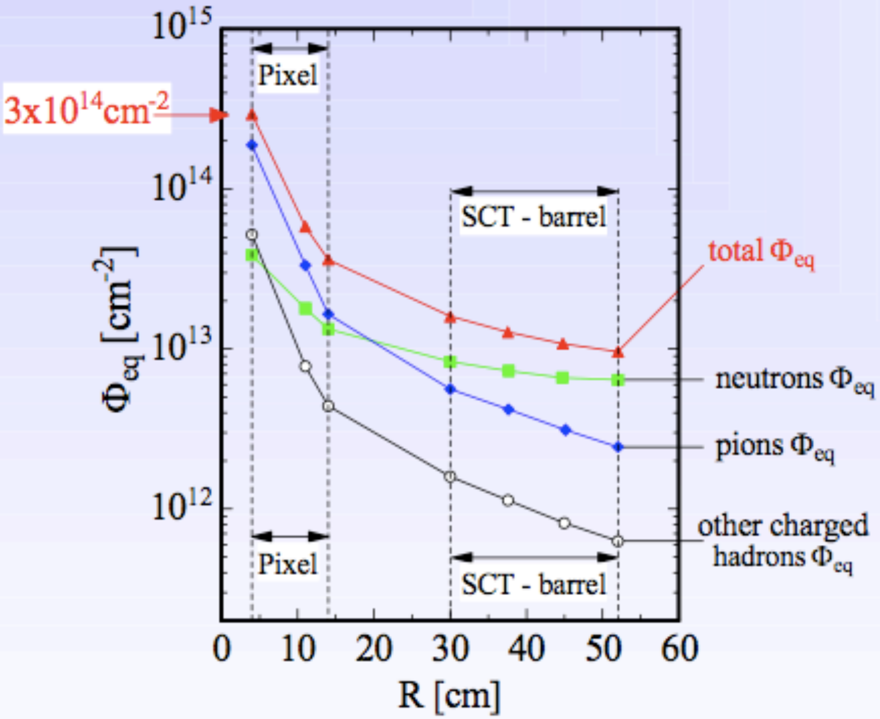

- Pixel detector: up to $\Phi_{eq} \approx 3.5 \cdot 10^{14}$ cm^{-2} /year
- Dominating type of particle is different for pixel (pions) and strip detectors (neutrons)

LHC silicon detectors:

- All detectors have been extensively tested and developed for radiation tolerance and are expected to survive the LHC radiation environment.
- Some experiments have already foreseen upgrades (e.g. LHCb Velo after 3 years).

Super LHC

- upgrade of LHC to 10 x higher Luminosity
  - ⇒ 10 x higher radiation levels
  - ⇒ Radiation damage will become a critical issue!
- ⇒ New, radiation tolerant detectors needed!

- What is radiation damage ?
- How to cope with it ?

from M. Moll

Radiation Damage

from M. Moll

- **Damage to the silicon crystal:** Displacement of lattice atoms

particle → Si_S — $E_K > 25$ eV →

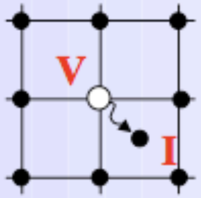

Vacancy + Interstitial ⟺ **"point defects", mobile in silicon, can react with impurities (O,C,..)**

$E_K > 5$ keV → **point defects and clusters of defects**

80 nm

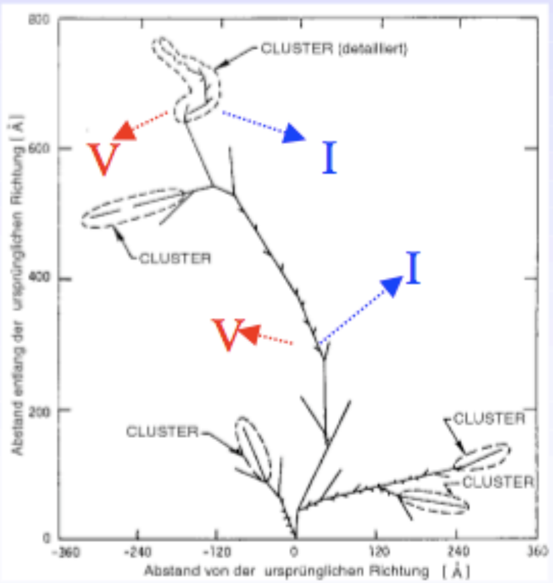

Distribution of vacancies created by a 50 keV Si-ion in silicon (typical recoil energy for 1 MeV neutrons):

← **Schematic** [Van Lint 1980]

Simulation [M.Huhtinen 2001] →

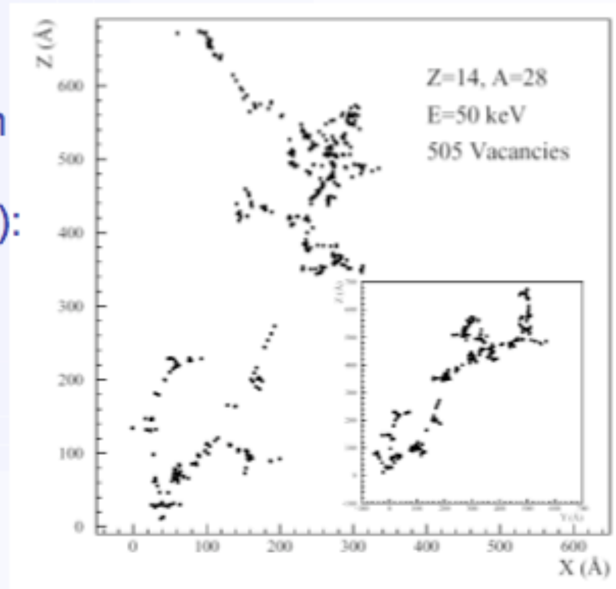

- **Defects can be electrically active (levels in the band gap)**
  - capture and release electrons and holes from conduction and valence band

  ⇒ can be charged - can be generation/recombination centers - can be trapping centers

Detector Aging

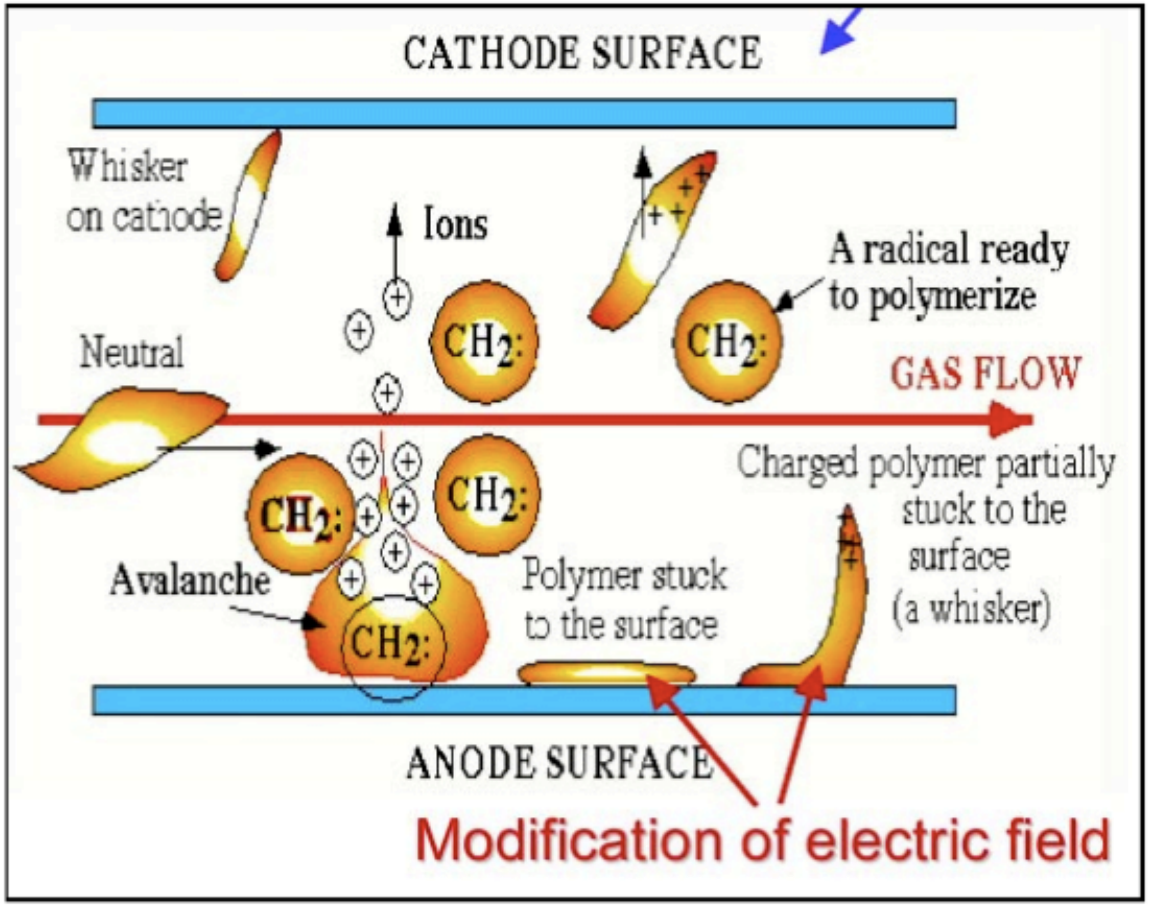

Complex plasma-chemical reactions in the avalanche can lead to polymerization.

Deposits on anode and cathode.

Deposits reduce electric field, which leads to reduced signal amplification (efficiency loss).

Malter effect:
Positive ions form a layer on cathode, high E-fields cause continuous electron extraction from cathode.
Leads to continuous discharge current.

Limitations of Gas Detectors

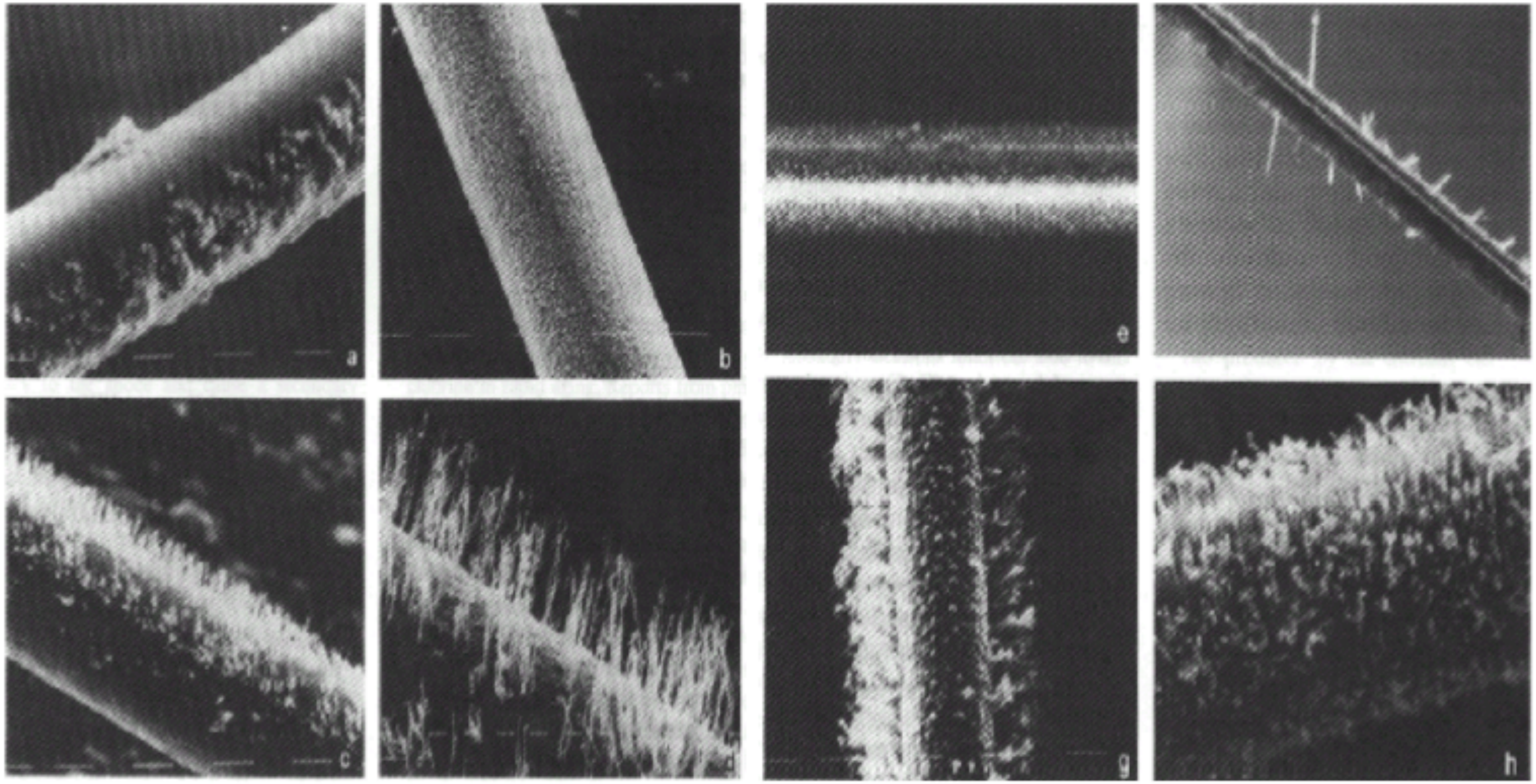

Wiskers are produced on the anode wire. They absorb the electrons. Thus electrons do not reach the main amplification region very close to the wire. This leads to efficiency loss.